

# *Tropical cyclone integrated kinetic energy in an ensemble of HighResMIP simulations*

Article

Accepted Version

Kreussler, P. ORCID: <https://orcid.org/0000-0003-4328-4712>,  
Caron, L.-P. ORCID: <https://orcid.org/0000-0001-5221-0147>,  
Wild, S. ORCID: <https://orcid.org/0000-0002-1089-5579>,  
Tomas, S. L., Chauvin, F. ORCID: <https://orcid.org/0000-0001-6071-7212>, Moine, M.-P., Roberts, M. J., Ruprich-Robert, Y.,  
Seddon, J. ORCID: <https://orcid.org/0000-0003-1302-1049>,  
Valcke, S. ORCID: <https://orcid.org/0000-0002-0438-5978>,  
Vanni re, B. and Vidale, P. L. ORCID: <https://orcid.org/0000-0002-1800-8460> (2021) Tropical cyclone integrated kinetic energy in an ensemble of HighResMIP simulations. *Geophysical Research Letters*, 48 (5). e2020GL090963. ISSN 1944-8007 doi: <https://doi.org/10.1029/2020gl090963>  
Available at <https://centaur.reading.ac.uk/96719/>

It is advisable to refer to the publisher's version if you intend to cite from the work. See [Guidance on citing](#).

To link to this article DOI: <http://dx.doi.org/10.1029/2020gl090963>

Publisher: American Geophysical Union (AGU)

All outputs in CentAUR are protected by Intellectual Property Rights law, including copyright law. Copyright and IPR is retained by the creators or other copyright holders. Terms and conditions for use of this material are defined in the [End User Agreement](#).

[www.reading.ac.uk/centaur](http://www.reading.ac.uk/centaur)

## **CentAUR**

Central Archive at the University of Reading

Reading's research outputs online

1 **Tropical Cyclone Precipitation in the HighResMIP Atmosphere-only**  
2 **Experiments of the PRIMAVERA Project**

3  
4  
5 Wei Zhang<sup>1,2\*</sup>, Gabriele Villarini<sup>1</sup>, Enrico Scoccimarro<sup>3</sup>, Malcolm Roberts<sup>4</sup>, Pier Luigi Vidale<sup>5</sup>,  
6 Benoit Vanniere<sup>5</sup>, Louis-Philippe Caron<sup>6</sup>, Dian Putrasahan<sup>7</sup>, Christopher Roberts<sup>8</sup>, Retish Senan<sup>8</sup>,  
7 and Marie-Pierre Moine<sup>9</sup>

8  
9  
10 <sup>1</sup> IIHR-Hydrosience & Engineering, The University of Iowa, Iowa City, Iowa, USA

11 <sup>2</sup>Department of Plants, Soils and Climate, Utah State University, Utah, USA

12 <sup>3</sup>Fondazione Centro Euro-Mediterraneo sui Cambiamenti Climatici, Bologna, Italy

13 <sup>4</sup>UK Meteorological Office, Exeter, UK

14 <sup>5</sup>National Centre for Atmospheric Science (NCAS), Department of Meteorology, University of  
15 Reading, Reading, UK

16 <sup>6</sup>Barcelona Supercomputing Center (BSC), Barcelona, Spain

17 <sup>7</sup>Max Planck Gesellschaft zur Foerderung der Wissenschaften E.V. (MPI-M), Hamburg, Germany

18 <sup>8</sup>European Centre for Medium-Range Weather Forecasts (ECMWF), Reading, UK

19 <sup>9</sup>Climat, Environnement, Couplages, Incertitudes (CECI), Universit'e de Toulouse, CNRS,  
20 Cerfacs, Toulouse, France

21  
22  
23 Revision submitted to

24 *Climate Dynamics*

25  
26 \*Corresponding author:

27 Wei Zhang, Ph.D.

28 Department of Plants, Soils and Climate, Utah State University, Utah, USA.

29 Email: w.zhang@usu.edu

30 Phone: (435) 791-1101

31

Abstract

32  
33 This study examines the climatology and structure of rainfall associated with tropical cyclones  
34 (TCs) based on the atmosphere-only Coupled Model Intercomparison Project Phase 6 (CMIP6)  
35 HighResMIP runs of the PRocess-based climate sIMulation: AdVances in high resolution  
36 modelling and European climate Risk Assessment (PRIMAVERA) Project during 1979-2014.  
37 We evaluate how the spatial resolution of climate models with a variety of dynamic cores and  
38 parameterization schemes affects the representation of TC rainfall. These HighResMIP  
39 atmosphere-only runs that prescribe historical sea surface temperatures and radiative forcings  
40 can well reproduce the observed spatial pattern of TC rainfall climatology, with high-resolution  
41 models generally performing better than the low-resolution ones. Overall, the HighResMIP  
42 atmosphere-only runs can also reproduce the observed percentage contribution of TC rainfall to  
43 total amounts, with an overall better performance by the high-resolution models. The models  
44 perform better over ocean than over land in simulating climatological total TC rainfall, TC  
45 rainfall proportion and TC rainfall per TC in terms of spatial correlation. All the models in the  
46 HighResMIP atmosphere-only runs underestimate the observed composite TC rainfall structure  
47 over both land and ocean, especially in their lower resolutions. The underestimation of rainfall  
48 composites by the HighResMIP atmosphere-only runs is also supported by the radial profile of  
49 TC rainfall. Overall, the increased spatial resolution generally leads to an improved model  
50 performance in reproducing the observed TC rainfall properties.

51



## 52 **1. Introduction**

53 Tropical cyclones (TCs) are associated with extreme rainfall and are responsible for  
54 extensive damages and numerous fatalities (e.g., Peduzzi et al. 2012; Rappaport 2014; Czajkowski  
55 et al. 2017; Klotzbach et al. 2018; Bosma et al. 2020). For example, Hurricanes Harvey and  
56 Florence serve to highlight the catastrophes that could be caused by extreme TC rainfall (e.g.,  
57 Emanuel 2017; Reed et al. 2018; Risser and Wehner 2017; Van Oldenborgh et al. 2017; Wang et  
58 al. 2018; Zhang et al. 2018) and are just two recent examples of a long list of catastrophic events.  
59 According to the National Oceanic and Atmospheric Administration (NOAA) National Center for  
60 Environmental Information (NCEI) (2020), there have been 44 TCs affecting the United States  
61 causing damage in excess of one billion dollars between 1980 and 2019; in total, these events  
62 caused \$945.9B (Consumer Price Index-Adjusted) and 6,502 fatalities.

63 Rainfall associated with TCs tends to be larger than for non-TC events. For instance, within  
64 the novel statistical framework of the Metastatistical Extreme Value Distribution, Miniussi et al.  
65 (2020) showed that the distribution of TC rainfall is different from the non-TC rainfall in the  
66 Eastern United States, especially for multi-day events, and that these storms tend to result in larger  
67 rainfall values. The impact of the TC rainfall is remarkable not only along the coastline, but also  
68 hundreds of miles inland in terms of flooding (e.g., Villarini et al. 2014a; Khouakhi et al. 2017;  
69 Aryal et al. 2018) and landslides (e.g., Bucknam et al. 2001). Despite these negative effects, they  
70 can also bring water critical for groundwater recharge, water supply and drought mitigation (e.g.,  
71 Abdalla and Al-Abri 2011; Kam et al. 2013; Zhang et al. 2017). It is therefore crucial that we  
72 improve our understanding of the processes and characteristics of TC rainfall, which could in turn  
73 lead to an improvement in its simulation and seasonal forecasting (e.g., Barlow 2011; Luitel et al.

74 2018; Liu et al. 2019; Prat and Nelson, 2016; Touma et al. 2019; Vecchi et al. 2019; Zhang et al.  
75 2019).

76         There are several drivers controlling TC rainfall, including low-level vertical wind shear  
77 (Corbosiero and Molinari 2003; Tang et al. 2014), terrain effects (DeHart and Houze Jr 2017;  
78 Nguyen et al. 2017), TC structure (Chen et al. 2006; Hence and Houze Jr 2012; Yu et al. 2017),  
79 sea surface temperature (Langousis and Veneziano 2009; Lin et al. 2015), and atmospheric  
80 aerosols (Wang et al. 2014; Zhao et al. 2018). Over the years and thanks to advances in observing  
81 capabilities, major progress has been made in understanding the temporal and spatial components  
82 of TC rainfall through satellite monitoring (e.g., Rios Gaona et al. 2018; Jiang and Zipser 2010;  
83 Jiang et al. 2011; Prat and Nelson 2013b), radar data (e.g., Villarini et al. 2011; Bao et al. 2017;  
84 Janapati et al. 2020) and rain gauges (e.g., Khouakhi et al. 2017; Villarini and Denniston 2016).  
85 Overall, these studies indicate that TC rainfall substantially contributes to the mean and extreme  
86 precipitation events, particularly along coastal regions (Khouakhi et al. 2017; Shepherd et al. 2007;  
87 Knight et al. 2009; Prat et al. 2013; Villarini et al. 2011; 2014b). In addition to observations,  
88 numerical models with the capability of resolving TCs have been used to examine TC rainfall (e.g.,  
89 Daloz et al. 2010; Kim et al. 2018; Liu et al. 2018; 2019; Moon et al. 2020; Scoccimarro et al.  
90 2014; 2017a; Villarini et al. 2014; Zhang et al. 2019). While climate models can well simulate the  
91 overall climatology of TC rainfall (e.g., Zhang et al. 2019), these models have limitations in  
92 simulating individual events and exhibit strong discrepancies in the simulated pattern and  
93 magnitude of TC rainfall (Scoccimarro et al. 2017c; Wright et al. 2015; Zhang et al. 2019).

94         In the climate modeling community, special attention has been paid to the examination of  
95 the impacts of horizontal resolution on TC simulations (e.g., Zhao et al. 2009; Caron et al. 2011;  
96 Manganello et al. 2012; Wehner et al. 2014; Roberts et al. 2015; 2020; Murakami et al. 2015;

97 Zhang et al. 2015; Vecchi et al. 2019). Despite these efforts, it is difficult to generalize the  
98 conclusions of these studies because of the differences in experimental design, tracking algorithm,  
99 and model parameters. While much of the focus has been on the role of resolution in terms of TC  
100 characteristics, recently Zhang et al. (2019) assessed the role of horizontal resolution of two  
101 climate models (i.e., the Geophysical Fluid Dynamics Laboratory (GFDL) Forecast-Oriented Low  
102 Ocean Resolution version of CM2.5 (FLOR, ~50km) and the High-Resolution FLOR (HiFLOR,  
103 ~25km)) in simulating TC rainfall and found that the high-resolution model (~25km) outperforms  
104 the low-resolution model (~50km) in reproducing and forecasting TC rainfall.

105         Based on this overview, numerical models have advanced our understanding of TC rainfall  
106 and provided insights into future projection of TC rainfall; however, there is a very limited number  
107 of climate models that can properly resolve TCs. Although there are individual studies that have  
108 focused on the impacts of horizontal resolution on TCs, there are many differences in the models'  
109 setups and simulations that would lead to the different behaviors in simulating TC rainfall,  
110 representing a critical obstacle in terms of the generalization of the results from different studies.  
111 Most conclusions drawn on the projection of TC rainfall are based on the fifth phase of the Coupled  
112 Model Intercomparison Project (CMIP5)'s climate models with spatial resolution of ~1-3 degrees,  
113 which are too coarse to properly resolve TCs. To overcome this limitation, the sixth phase of the  
114 Coupled Model Intercomparison Project (CMIP6) High Resolution Model Intercomparison  
115 Project (HighResMIP) provides multi-model and multi-resolution simulations to the scientific  
116 community (Haarsma et al. 2016). Using the CMIP6 HighResMIP protocol, the European Union  
117 Horizon 2020's PROcess-based climate sIMulation: AdVances in high resolution modelling and  
118 European climate Risk Assessment (PRIMAVERA) project has contributed global atmospheric  
119 general circulation models (AGCM) simulations at a CMIP6-type resolution (i.e., ~100 km) and

120 higher (e.g., ~25 km), which allow us to examine TCs and understand the robustness of changes  
121 in TC rainfall across a wide range of numerical models and spatial resolutions (Roberts et al. 2020).  
122 Roberts et al. (2020) examined the roles of horizontal resolution in simulating TCs in terms of  
123 frequency, intensity, structure and accumulated cyclone energy across these models. In addition,  
124 Vanniere et al. (2020) focused on the sensitivity of moisture budget associated with TC rainfall to  
125 different spatial resolution of the climate models in this project. This study will take advantage of  
126 the simulations archived in the PRIMAVERA project to evaluate the fidelity of these climate  
127 models in representing TC rainfall and the dependence of skill on resolution.

128 The remainder of the manuscript is organized as follows. Section 2 describes data and  
129 methods, followed by Section 3 that presents results based on observations and models. Finally,  
130 Section 4 summarizes the main points and concludes the study.

131

## 132 **2. Data and Methods**

133 TC observations are obtained from the International Best Track Archive for Climate  
134 Stewardship (IBTrACS) version 4 with longitude, latitude, time, intensity (i.e., maximum  
135 sustained wind) and central pressure at the six-hour time scale (Knapp et al. 2010). Rainfall is  
136 obtained from the Multi-Source Weighted-Ensemble Precipitation, version 2 (MSWEP V2) which  
137 is a gridded precipitation dataset available during 1979–2017 with high spatial ( $0.1^\circ$ ) and temporal  
138 (three-hour) resolution (Beck et al. 2017a,b). TC rainfall is defined as the rainfall at 6-hour  
139 intervals within a 500-km radius of a TC center by accounting for the rainfall covering the inner  
140 core of the TC and the adjacent rainbands (e.g., Dare et al. 2012; Villarini et al. 2014b; Zhang et  
141 al. 2019). Although there might be some uncertainties in extracting TC rainfall using this radius at  
142 each 6-hour time step, the selection of this radius is also supported by the fact that most

143 precipitation associated with TCs occurs within  $5^\circ$  (~500km) from the center of the storm for  
144 climate models (Trenberth et al. 2007; Vanniere et al. 2020). The TC-rainfall composites are the  
145 composites of the extracted TC rainfall using the 500-km radius and we process the TC rainfall for  
146 three scenarios: land and ocean, only land and only ocean.

147 We use the HighResMIP atmosphere-only simulations performed by the Met Office  
148 Hadley Centre's HadGEM3-GC313-GC31 (Roberts et al. 2019a), the European Centre for  
149 Medium-Range Weather Forecasts Integrated Forecasting System (ECMWF IFS) (Roberts et al.  
150 2018), CNRM-CM6-1 developed by Centre National de Recherches Météorologiques—Groupe  
151 d'études de l'Atmosphère Météorologique/Centre Européen de Recherche et de Formation  
152 Avancée (Voltaire et al. 2019), the Fondazione Centro Euro-Mediterraneo sui Cambiamenti  
153 Climatici Climate Model Version 2 (CMCC-CM2-(V)HR4; Cherchi et al. 2019, Scoccimarro et  
154 al. 2020), the EC-EARTH3 Consortium's EC-Earth3P (Haarsma et al. 2019), and Max Planck  
155 Institute Earth System Model version 1.2 (MPI-ESM1-2; Gutzjahr et al. 2019) (see Table 1 for  
156 details). The atmosphere-only HighResMIP experiments are forced by the historical estimates of  
157 sea surface temperature, sea ice, and radiative forcings (as described in Haarsma et al. 2016). It  
158 should be noted that the atmosphere-only HighResMIP simulations are slightly different from the  
159 CMIP6 (Eyring et al. 2016) AMIP experiments (Gates et al. 1999) in terms of forcing of aerosol,  
160 sea surface temperature and sea ice (Roberts et al. 2020). We obtain the model simulations  
161 archived in the Earth System Grid Federation (ESGF) nodes, including Roberts (HadGEM3-  
162 GC31; 2017a, 2017b, 2017c), Roberts et al. (ECMWF-IFS; 2017a, 2017b), Voltaire (CNRM-  
163 CM6-1; 2017, 2018), Scoccimarro et al. (CMCC-CM2-(V)HR4; 2017b, 2017c), EC-Earth  
164 Consortium (EC-Earth3P; 2018a, 2018b), and von Storch et al. (MPI-ESM1-2; 2017, 2019). In  
165 addition, the TC tracks obtained from these datasets are available from Roberts (2019b).

166 To facilitate the comparison of the simulation of TC rainfall, the climate model outputs are  
167 grouped into high-, medium- and low- spatial-resolution models (Table 1). While ECMWF IFS  
168 data provided to the HighResMIP simulations are based on a reduced-resolution regular grid, the  
169 original ECMWF-IFS output uses the cubic octahedral reduced Gaussian grid, with resolutions of  
170 Tco399 (~25 km) and Tco199 (~50 km) for the HR and LR configurations, respectively. Therefore,  
171 we include ECMWF-IFS-HR/ECMWF-IFS-LR in the high-resolution/middle-resolution group,  
172 respectively (Table 1). TC tracks with latitude, longitude, time and intensity are derived by  
173 applying a tracker called “TRACK” to the simulations performed by these models (Hodges et al.  
174 2017). This tracker uses the 6-hourly relative vorticity at the 850-, 700-, and 600-hPa levels for  
175 tracking TCs and has been widely used in TC studies (Hodges et al. 2017).

176 We evaluate the performance of these models in simulating TC rainfall across the globe,  
177 and for the basins (Table 2): western North Pacific, eastern North Pacific, North Atlantic, South  
178 Atlantic, North Indian Ocean, South-West Indian Ocean and South Pacific & Australia. We use  
179 spatial correlation and root mean square error (RMSE) as quantitative metrics for the evaluation.  
180 Because there is no named storm in South Atlantic in observations during the study period (Table  
181 S1), we do not include the analysis of spatial correlation and RMSE between observations and  
182 models for this basin.

183 Beyond the high resolution of these models, a major advantage of the PRIMAVERA  
184 Project is the consistency of the simulations and outputs: all the models were run using the same  
185 forcings, and the tracking of the storms is the same across models, allowing for a direct comparison  
186 in terms of model performance and on the role of resolution.

187

### 188 **3. Results**

### 189 3.1 Total TC rainfall

190 The annual total TC rainfall averaged over 1979-2014 in the observations exhibits regional  
191 differences across ocean basins (Figure 1). For example, the annual TC rainfall is the highest in  
192 the western North Pacific, followed by the eastern North Pacific. The annual TC rainfall in the  
193 North Atlantic is lower than in the eastern North Pacific and little TC rainfall is observed in the  
194 South Atlantic (Figure 1). Qualitatively, the climate models tend to capture the overall spatial  
195 climatological pattern of TC rainfall in the observations; this is particularly true in relation to the  
196 areas in the North Pacific characterized by larger TC rainfall values compared to the rest of the  
197 basins (Figure 2). The GCMs generally produce spurious TC rainfall in the South Atlantic (Figure  
198 2). Specifically, CMCC-CM2-VHR4, EC-Earth3P-HR, ECMWF-IFS-HR, and ECMWF-IFS-LR  
199 reproduce well the total TC rainfall amount across different basins (Figure 2), consistent with  
200 spatial correlation and RMSE between observed and simulated total TC rainfall (Tables 3-4). In  
201 addition, CNRM-CM6-1-HR, CNRM-CM6-1, HadGEM3-GC31-HM, HadGEM3-GC31-MM,  
202 HadGEM3-GC31-LM point to an overestimation of the total TC rainfall, while EC-Earth3P,  
203 MPIESM1-2-XR and MPIESM1-2-HR to an underestimation of the total TC rainfall across all  
204 basins (Figure 2). This is consistent with the results of TC track density (Figure 3), which is also  
205 documented in Roberts et al. (2020) which reported that EC-Earth3P and MPIESM1-2-XR  
206 underestimate TC track density. Vanniere et al. (2020) also found that TC activity/frequency plays  
207 an important role in explaining the differences in total TC rainfall between high-resolution and  
208 low-resolution models. Based on the above results, high-resolution models tend to perform better  
209 in reproducing the observed climatology of TC rainfall. Overall, increase in model resolution tends  
210 to produce a higher amount of total TC rainfall for the CMCC models, EC-Earth3P models,  
211 HadGEM3-GC31 (i.e., HadEM3-GC31-HM and HadGEM3-GC31-LM) and ECMWF-IFS

212 models, while TC rainfall shows little to no sensitivity to spatial resolution in CNRM-CM6-1 and  
213 MPIESM1-2 models (Figure 2). Four of the six models exhibit remarkable differences in TC  
214 rainfall between high-resolution and low-resolution models while the other two show similar  
215 results (Figure 2). The low sensitivity to spatial resolution in CNRM-CM6-1 and MPIESM1-2  
216 models may be due to low absolute resolution in the models, the high-resolution version of which  
217 is around ~50km (Table 1).

### 218 **3.2 Contribution of TC rainfall to Total Rainfall**

219 In addition to total TC rainfall, we also examine the percentage contribution of TC rainfall  
220 to total rainfall. In the observations, the percentage contribution presents remarkable regional  
221 differences with the highest values in the western and eastern North Pacific (Figure 4), consistent  
222 with total TC rainfall (Figure 1). Climate models exhibit strong discrepancies in the capability of  
223 reproducing the observed percentage contribution (Figure 4). Globally, EC-Earth3P-HR,  
224 ECMWF-IFS-HR, ECMWF-IFS-LR, HadGEM3-GC31-HM, HadGEM3-GC31-MM, and  
225 HadGEM3-GC31-LM reproduce well the observed contribution of TC rainfall in terms of RMSE.  
226 CMCC-CM2-VHR4, EC-Earth3P-HR, EC-Earth3P, ECMWF-IFS-HR, ECMWF-IFS-LR, and  
227 HadGEM3-GC31 models produce spatial correlations greater than 0.8, suggesting a good  
228 performance (Table 5). The models exhibit marked regional differences. For example, CNRM-  
229 CM6-1-HR and CNRM-CM6-1 reproduce well the observed contribution of TC rainfall in the  
230 western North Pacific, and the performance of these models is not very promising in the North  
231 Indian Ocean (Figure 4 and Tables 5-6). High-resolution models generate a higher contribution,  
232 more similar to the observations except for MPIESM1-2-XR/MPIESM1-2-HR and CNRM-CM6-  
233 1-HR/CNRM-CM6-1, which produce similar percentage contributions between high-resolution  
234 and low-resolution models (Figure 4). Therefore, most of the high-resolution models perform



235 better than their low-resolution counterparts in reproducing the global fractional contribution  
236 (Figure 4 and Table 5). To further understand the proportion of TC rainfall, we also examine the  
237 bias in the models (Figure 5). Overall, the bias in TCR proportion (Figure 5) is mainly due to the  
238 bias in TC rainfall (Figure 2), rather than total precipitation (Figure 6).

### 239 **3.3 TC rainfall per track density**

240 All the models in the PRIMAVERA Project underestimate the amount of TC rainfall per  
241 track density (i.e., total TC rainfall divided by track density) in the observations (Figure 7).  
242 Therefore, given that the TC rainfall amounts identified in the models were similar to the  
243 observations, it means that there are generally more storms in the models than in the observational  
244 records. As we compare the results between the different resolutions of the models, some models  
245 (i.e., CMCC-CM2, CNRM and HadGEM3-GC31) have a tendency for lower-resolution versions  
246 to have larger per-TC rainfall amounts. This counter-intuitive results may be due to the fact that  
247 lower TC density is produced by low-resolution simulations than in the high-resolution ones  
248 (Figure 3), consistent with Vanniere et al. (2020) showing that rainfall per TC is biased high in  
249 low-resolution models. The spatial correlation between observed and simulated amount of TC  
250 rainfall per track density (Table S2) is lower than for total TC rainfall or fractional contribution,  
251 with most of the correlation coefficients that are not statistically significant. Among the models  
252 used in this study, the CNRM models perform the best in simulating the rainfall per track density  
253 (Figure 7 and Tables S2-3) and this is consistent with the fact that CNRM performs well in  
254 simulating the strongest TCs (Roberts et al. 2020).

### 255 **3.4 TC rainfall over Ocean and Land**

256 We also evaluate the performance of the models in simulating climatological TC rainfall  
257 over ocean and land. Overall, the models perform better in simulating total TC rainfall, TC rainfall

258 proportion and TC rainfall per TC over ocean than over land in terms of spatial correlation (Tables  
259 S4-6). However, the models generate a larger RMSE for the three metrics over ocean than over  
260 land (Tables S4-6), and this may be due to a large climatology of TC rainfall over ocean (Figure  
261 1).

### 262 **3.5 Composites and Profile of TC rainfall**

263 We process the composite TC rainfall (within the 500-km radius of TC center) at 6-hour  
264 time step for all the storms, those in the northern hemisphere and those in the southern hemisphere  
265 in observations and climate models (Figure 8). The composite TC rainfall (within the 500-km  
266 radius) at 6-hourly intervals in the observations is higher than model simulations over ocean and  
267 land (Figure 8). CMCC-CM2-VHR4 performs the best in reproducing the composite TC rainfall  
268 over ocean and land, with larger precipitation values closer to the center of circulation of the  
269 storms, even though the size of the TCs tends to be smaller than in the observations and in other  
270 models (e.g., CNRM). There is also a tendency for the storms in the northern hemisphere to exhibit  
271 larger rainfall values compared to those in the southern hemisphere, consistent with the  
272 observations. The high-resolution models produce larger composite TC rainfall rate than low-  
273 resolution models, which tend to spread rainfall over larger distances from the center of circulation  
274 of the TCs (Figure 8). In addition, we compare the composite rainfall in the 200 strongest storms  
275 in observations and the low- and high-resolution models. Overall, the composite rainfall rate in the  
276 high-resolution models is larger than in the low-resolution ones except for the MPI-ESM 1-2  
277 models that simulate similar composite TC rainfall (Figure 9). The differences in composite TC  
278 rainfall of the 200 strongest TCs between low-resolution and high-resolution models (Figure 9)  
279 are more remarkable than the results for all TCs (Figure 8), and this may be due to a large portion  
280 of intense TCs in the high-resolution models than low-resolution ones (Roberts et al. 2020). To

281 assess whether the models' skill is different in simulating TC rainfall over ocean or land mass, we  
282 examine the composite TC rainfall over ocean and land, separately. The composite TC rainfall  
283 over the ocean exhibits similar characteristics as those over land & ocean, with a well-defined  
284 center of circulation, albeit presenting a slightly higher magnitude (Figure 10). While almost all  
285 the models underestimate the composite TC rainfall over land compared with observations (Figure  
286 11), CMCC-CM2-VHR4 slightly overestimates the center of composite TC rainfall over land and  
287 HadGEM3-GC31-HM produces a similar magnitude of composite TC rainfall over land (Figure  
288 11). Given the fact that TCs in models have a shorter path on land than the observations (due to  
289 the tracker) and TC rainfall rate over ocean is larger than over land, this suggests that the  
290 underestimation of composite TC rainfall in models might be even more pronounced than the  
291 results here. Based on these results, there are no large differences in the performance of the models  
292 in reproducing composite TC rainfall over ocean or land. Note that the composite rainfall patterns  
293 are consistent with the results in Kim et al. (2018) which examined the composite TC rainfall  
294 across a family of Geophysical Fluid Dynamics Laboratory (GFDL) models.

295 In addition to the examination of the composite TC rainfall, we compute the radial profile  
296 of TC rainfall across different models grouped by spatial resolution (Table 1) and land/ocean  
297 masks (Figure 12). Consistent with the results in Figures 8-11, the observed rainfall tends to be  
298 higher than what is generated by these models, especially closer to their center of circulation; this  
299 statement is valid regardless of resolution, and whether over land or ocean. The observed TC  
300 rainfall over the oceans tends to peak within 100 km from the center of the storm, and then to  
301 rapidly decrease as we move further away. This feature is generally well captured by the models,  
302 with the CMCC-CM2-VHR4 tending to perform the best among high-resolution groups. Among  
303 the mid-resolution group, HadGEM3-GC31-MM exhibits the highest skill in simulating the radial

304 profile of TC rainfall, while CNRM-CM6-1 tends to perform the best among the low-resolution  
305 group (Figure 12). The model performance in terms of TC rainfall when the storms are over land  
306 is similar to that mentioned for the storms over the ocean, even though the rainfall amounts tend  
307 to be smaller and to decrease more slowly as they progress inland. The radial profile of TC rainfall  
308 is consistent with Kim et al. (2018) and Moon et al. (2020) in terms of pattern and magnitude of  
309 TC rainfall across different climate models.

310

#### 311 **4. Conclusion**

312 TC rainfall has been a challenge for climate modeling community because this metric is  
313 associated with TC genesis, track, and intensity. By taking advantage of the European Union  
314 Horizon 2020's PRIMAVERA Project, we have examined the skill of state-of-the-art global  
315 climate models in reproducing several aspects of the rainfall associated with these storms in  
316 HighResMIP atmosphere-only experiments and assessed the dependence of the skill on model  
317 resolution.

318 In general, high-resolution models perform better than their lower resolution counterparts  
319 in reproducing several characteristics of the TC distribution. They tend to provide a more realistic  
320 representation of the observations both in terms of patterns and amounts, except for average TC  
321 rainfall per track density for which low-resolution models seem better for some models. The  
322 simulation of TC rainfall by these models exhibits remarkable regional differences and  
323 discrepancies. For example, the CMCC-CM2 and ECMWF-IFS models reproduce the total TC  
324 rainfall found in observations, while they slightly underestimate their percentage contribution and  
325 overall amount per track density. By contrast, CNRM-CM6-1 and HadGEM3-GC31 models  
326 overestimate total TC rainfall, but they reproduce the fractional contribution of TC rainfall to total

327 rainfall. MPIESM1-2 and EC-Earth3P models underestimate most of the metrics associated with  
328 TC rainfall. Overall, the models perform better in simulating climatological total TC rainfall, TC  
329 rainfall proportion and TC rainfall per TC over ocean than over land in terms of spatial correlation.  
330 However, the models generate larger RMSE for the three metrics over ocean than over land,  
331 probably due to a larger climatology of TC rainfall over ocean.

332         When we stratified the results of composite TC rainfall across land and ocean, we did not  
333 find any large changes in performance of these models, as they were able to reproduce the overall  
334 patterns albeit with lower rainfall magnitudes. Overall, CMCC-CM2-VHR4 performs the best in  
335 simulating the radial profile of TC rainfall among the high-resolution model group, while  
336 HadGEM3-GC31-MM (CNRM-CM6-1) exhibits the highest skill in simulating the radial profile  
337 of TC rainfall in the mid-resolution (low-resolution) group.

338         While most models tend to improve their performance as we increase their horizontal  
339 resolution, the CNRM-CM6-1 and MPIESM1-2 models are two exceptions, producing similar  
340 results in their low- and high- resolution versions. Such similar performances between high-  
341 resolution and low-resolution climate models need to be further investigated from the perspective  
342 of convection, circulation and TC dynamics. For example, Vanniere et al (2020) investigated  
343 possible mechanisms by examining moisture budget, and found that the distribution of  
344 precipitation per TC averaged in a 5-degree radial cap does not change significantly, which can be  
345 explained by the large-scale balance that shapes the moisture budget of TCs.

346         In summary, our findings indicate that the investment in performing the high-resolution  
347 simulations with these models has been paid off in terms of the gained realism in reproducing TC  
348 rainfall. As we increase the horizontal resolution and we improve the description of the processes

349 at play, we expect to further improve the simulation of these storms, providing basic information  
350 towards our preparation, mitigation and response efforts.

351  
352

353 **Acknowledgements:**

354

355 We thank the two anonymous reviewers for insightful comments. Wei Zhang and Gabriele

356 Villarini acknowledge support by the National Science Foundation under Grant EAR-1840742.

357 MR, LPC, CDR, RS, PLV, ES, BV, DP, and MPM acknowledge funding from the PRIMAVERA

358 project, funded by the European Union's Horizon 2020 programme under Grant Agreement no.

359 641727.

360

361 **Reference:**

- 362
- 363 Abdalla, O., and R. bin Y. Al-Abri, (2011). Groundwater recharge in arid areas induced by  
364 tropical cyclones: lessons learned from Gonu 2007 in Sultanate of Oman. *Environ Earth Sci*,  
365 63, 229–239. <https://doi.org/10.1007/s12665-010-0688-y>
- 366 Aryal, Y.N., G. Villarini, W. Zhang, and G.A. Vecchi, Long term changes in flooding and heavy  
367 rainfall associated with North Atlantic tropical cyclones: Roles of the North Atlantic  
368 Oscillation and El Niño-Southern Oscillation, *Journal of Hydrology*, 559, 698-710, 2018.
- 369 Bao, X., D. Wu, X. Lei, L. Ma, D. Wang, K. Zhao, and B. J.-D. Jou, 2017: Improving the  
370 extreme rainfall forecast of Typhoon Morakot (2009) by assimilating radar data from Taiwan  
371 Island and mainland China. *Journal of Meteorological Research*, **31**, 747-766.
- 372 Barlow, M., 2011: Influence of hurricane-related activity on North American extreme  
373 precipitation. *Geophysical Research Letters*, 38 , L04705.
- 374 Beck, H. E., A. I. Van Dijk, V. Levizzani, J. Schellekens, D. Gonzalez Miralles, B. Martens, and  
375 A. De Roo, 2017a: MSWEP: 3-hourly 0.25 global gridded precipitation (1979-2015) by  
376 merging gauge, satellite, and reanalysis data. *Hydrology and Earth System Sciences*, **21**, 589-  
377 615.
- 378 Bosma, C. D., D. B. Wright, P. Nguyen, J. P. Kossin, D. C. Herndon, and J. M. Shepherd, 2020:  
379 An intuitive metric to quantify and communicate tropical cyclone rainfall hazard. *Bulletin of*  
380 *the American Meteorological Society*, 101, E206-E220.
- 381 Beck, H. E., and Coauthors, 2017b: Global-scale evaluation of 22 precipitation datasets using  
382 gauge observations and hydrological modeling. *Hydrology and Earth System Sciences*, **21**,  
383 6201.
- 384 Bucknam, R. C., J.A. Coe, M.M. Chavarria, J.W. Godt, A.C. Tarr, ... , and M.L. Johnson (2001).  
385 Landslides triggered by Hurricane Mitch in Guatemala - Inventory and discussion. USGS  
386 Report Number 2001-443.
- 387 Caron, L-P, CG Jones and K Winger (2011) Impact of resolution and downscaling technique in  
388 simulating recent Atlantic tropical cyclone activity. *Climate Dynamics*, 5, 869-892. doi:  
389 10.1007/s00382-010-0846-7.
- 390 Chavas, D. R., N. Lin, W. Dong, and Y. Lin (2016), Observed Tropical Cyclone Size Revisited,  
391 *Journal of Climate*, 29(8), 2923-2939, doi:10.1175/jcli-d-15-0731.1.
- 392 Chen, S. S., J. A. Knaff, and F. D. Marks Jr, 2006: Effects of vertical wind shear and storm  
393 motion on tropical cyclone rainfall asymmetries deduced from TRMM. *Monthly Weather*  
394 *Review*, **134**, 3190-3208.
- 395 Cherchi, A., and Coauthors, 2019: Global Mean Climate and Main Patterns of Variability in the  
396 CMCC-CM2 Coupled Model. *Journal of Advances in Modeling Earth Systems*, **11**, 185-209.
- 397 Corbosiero, K. L., and J. Molinari, 2003: The relationship between storm motion, vertical wind  
398 shear, and convective asymmetries in tropical cyclones. *Journal of the Atmospheric Sciences*,  
399 **60**, 366-376.
- 400 Czajkowski, J., G. Villarini, M. Montgomery, E. Michel-Kerjan, and R. Goska, Assessing  
401 current and future freshwater flood risk from North Atlantic tropical cyclones via insurance  
402 claims, *Scientific Reports*, 7, 1-10, 2017.
- 403 Daloz, A. S., F. Chauvin, and F. Roux, 2010: Tropical cyclone rainfall in the observations,  
404 reanalysis and ARPEGE simulations in the North Atlantic Basin. *Hurricanes and climate*  
405 *change*, Springer, 57-79.

406 Dare, R. A., N. E. Davidson, and J. L. McBride, 2012: Tropical cyclone contribution to rainfall  
407 over Australia. *Monthly Weather Review*, **140**, 3606-3619.

408 DeHart, J. C., and R. A. Houze Jr, 2017: Orographic modification of precipitation processes in  
409 Hurricane Karl (2010). *Monthly Weather Review*, **145**, 4171-4186.

410 EC-Earth Consortium (EC-Earth), 2018a: EC-Earth-858 Consortium EC-Earth3P model output  
411 prepared for CMIP6 HighResMIP. Earth System Grid Federation. <http://cera860>  
412 [www.dkrz.de/WDCC/meta/CMIP6/CMIP6.HighResMIP.EC-Earth-Consortium.EC861Earth3P](http://www.dkrz.de/WDCC/meta/CMIP6/CMIP6.HighResMIP.EC-Earth-Consortium.EC861Earth3P)

413 EC-Earth Consortium (EC-Earth), 2018b: EC-Earth-Consortium EC-Earth3P-HR model output  
414 prepared for CMIP6 HighResMIP. Earth System Grid Federation. <http://cera->  
415 [www.dkrz.de/WDCC/meta/CMIP6/CMIP6.HighResMIP.EC-Earth-Consortium.EC-Earth3P-](http://www.dkrz.de/WDCC/meta/CMIP6/CMIP6.HighResMIP.EC-Earth-Consortium.EC-Earth3P-HR)  
416 HR

417 Emanuel, K., 2017: Assessing the present and future probability of Hurricane Harvey's rainfall.  
418 *Proceedings of the National Academy of Sciences*, **114**, 12681-12684.

419 Gates, W. L., and Coauthors, 1999: An overview of the results of the Atmospheric Model  
420 Intercomparison Project (AMIP I). *Bulletin of the American Meteorological Society*, **80**, 29-  
421 56.

422 Gutjahr, O., and Coauthors, 2019: Max Planck Institute Earth System Model (MPI-ESM1.2) for  
423 the High-Resolution Model Intercomparison Project (HighResMIP). *Geosci. Model Dev.*, **12**,  
424 3241-3281.

425 Haarsma, R. J., and Coauthors, 2016: High Resolution Model Intercomparison Project  
426 (HighResMIP v1.0) for CMIP6. *Geosci. Model Dev.*, **9**, 4185-4208.

427 Hence, D. A., and R. A. Houze Jr, 2012: Vertical structure of tropical cyclone rainbands as seen  
428 by the TRMM Precipitation Radar. *Journal of the atmospheric sciences*, **69**, 2644-2661.

429 Hodges, K., A. Cobb, and P. L. Vidale, 2017: How well are tropical cyclones represented in  
430 reanalysis datasets? *Journal of Climate*, **30**, 5243-5264.

431 Janapati, J., and Coauthors, 2020: Raindrop Size Distribution Characteristics of Indian and  
432 Pacific Ocean Tropical Cyclones Observed at India and Taiwan Sites. *Journal of the*  
433 *Meteorological Society of Japan. Ser. II.*

434 Jiang, H., and E. J. Zipser, 2010: Contribution of tropical cyclones to the global precipitation  
435 from eight seasons of TRMM data: Regional, seasonal, and interannual variations. *Journal of*  
436 *climate*, **23**, 1526-1543.

437 Jiang, H., C. Liu, and E. J. Zipser, 2011: A TRMM-based tropical cyclone cloud and  
438 precipitation feature database. *Journal of applied meteorology and climatology*, **50**, 1255-  
439 1274.

440 Kam, J., J. Sheffield, X. Yuan, and E. F. Wood, 2013: The Influence of Atlantic Tropical  
441 Cyclones on Drought over the Eastern US (1980-2007), *J. Climate*, 26 (10), 3067-3086.

442 Kim, D., and Coauthors, 2018: Process-oriented diagnosis of tropical cyclones in high-resolution  
443 GCMs. *Journal of Climate*, 31, 1685-1702.

444 Khouakhi, A., G. Villarini, and G. A. Vecchi, 2017: Contribution of tropical cyclones to rainfall  
445 at the global scale. *Journal of Climate*, **30**, 359-372.

446 Klotzbach, P.J., S.G. Bowen, R. Pielke Jr., and M. Bell, Continental U.S. hurricane landfall  
447 frequency and associated damage: Observations and future risks, *Bulletin of the American*  
448 *Meteorological Society*, 99(7), 1359-1376, 2018.

449 Knapp, K. R., M. C. Kruk, D. H. Levinson, H. J. Diamond, and C. J. Neumann, 2010: The  
450 International Best Track Archive for Climate Stewardship (IBTrACS). *Bulletin of the*  
451 *American Meteorological Society*, **91**, 363-376.



452 Knight, D. B., and R. E. Davis, 2009: Contribution of tropical cyclones to extreme rainfall events  
453 in the southeastern United States. *Journal of Geophysical Research: Atmospheres*, **114**.

454 Lin, Y., M. Zhao, and M. Zhang, 2015: Tropical cyclone rainfall area controlled by relative sea  
455 surface temperature. *Nature communications*, **6**, 1-7.

456 Liu, M., G. A. Vecchi, J. A. Smith, and H. Murakami, 2018: Projection of landfalling–tropical  
457 cyclone rainfall in the Eastern United States under anthropogenic warming. *Journal of*  
458 *Climate*, **31**, 7269-7286.

459 Liu, M., G. A. Vecchi, J. A. Smith, and T. R. Knutson, 2019: Causes of large projected increases  
460 in hurricane precipitation rates with global warming. *npj Climate and Atmospheric Science*,  
461 **2**, 38.

462 Luitel, B., G. Villarini, and G.A. Vecchi, Verification of the skill of numerical weather  
463 prediction models in forecasting rainfall from U.S. landfalling tropical cyclones, *Journal of*  
464 *Hydrology*, 556, 1026-1037, 2018.

465 Manganello, J. V., and Coauthors, 2012: Tropical cyclone climatology in a 10-km global  
466 atmospheric GCM: toward weather-resolving climate modeling. *Journal of Climate*, **25**,  
467 3867-3893.

468 Miniussi, A., G. Villarini, and M. Marani, Analyses through the metastatistical extreme value  
469 distribution identify contributions of tropical cyclones to rainfall extremes in the eastern US,  
470 *Geophysical Research Letters*, 47(7), e2020GL087238, 1-9, 2020.

471 Moon, Y., and Coauthors, 2020: Azimuthally averaged wind and thermodynamic structures of  
472 tropical cyclones in global climate models and their sensitivity to horizontal resolution.  
473 *Journal of Climate*, **33**, 1575-1595.

474 Murakami, H., and Coauthors, 2015: Simulation and prediction of category 4 and 5 hurricanes in  
475 the high-resolution GFDL HiFLOR coupled climate model. *Journal of Climate*, **28**, 9058-  
476 9079.

477 Nguyen, L. T., R. F. Rogers, and P. D. Reasor, 2017: Thermodynamic and kinematic influences  
478 on precipitation symmetry in sheared tropical cyclones: Bertha and Cristobal (2014). *Monthly*  
479 *Weather Review*, **145**, 4423-4446.

480 NOAA National Centers for Environmental Information (NCEI) U.S. Billion-Dollar Weather  
481 and Climate Disasters (2020). <https://www.ncdc.noaa.gov/billions/>, DOI: 10.25921/stkw-  
482 7w73

483 Peduzzi, P., B. Chatenoux, H. Dao, A. De Bono, C. Herold, J. Kossin, F. Mouton, and O.  
484 Nordbeck, Global trends in tropical cyclone risk, *Nature Climate Change*, **2**, 289-294, 2012.

485 Prat, O. P., and B. R. Nelson, 2013a: Precipitation contribution of tropical cyclones in the  
486 southeastern United States from 1998 to 2009 using TRMM satellite data. *Journal of*  
487 *Climate*, **26**, 1047-1062.

488 —, 2013b: Mapping the world's tropical cyclone rainfall contribution over land using the  
489 TRMM Multi-satellite Precipitation Analysis. *Water Resources Research*, **49**, 7236-7254.

490 —, 2016: On the link between tropical cyclones and daily rainfall extremes derived from  
491 global satellite observations. *Journal of Climate*, **29**, 6127-6135.

492 Rappaport, E.N., Fatalities in the United States from Atlantic tropical cyclones, 2014: New data  
493 and interpretation, *Bulletin of the American Meteorological Society*, **95(3)**, 341-346.

494 Reed, K. A., A. Standfield, M. F. Wehner, and C. M. Zarzycki, 2018: The human influence on  
495 Hurricane Florence. *website accessed October*.

496 Rios Gaona, M.F., G. Villarini, W. Zhang, and G.A. Vecchi, The added value of IMERG in  
497 characterizing rainfall in tropical cyclones, *Atmospheric Research*, **209**, 95-102, 2018.

498 Risser, M. D., and M. F. Wehner, 2017: Attributable human-induced changes in the likelihood  
499 and magnitude of the observed extreme precipitation during Hurricane Harvey. *Geophysical*  
500 *Research Letters*, **44**, 12,457-412,464.

501 Roberts, C. D., R. Senan, F. Molteni, S. Boussetta, M. Mayer, and S. P. Keeley, 2018: Climate  
502 model configurations of the ECMWF-Integrated Forecasting System (ECMWF-IFS cycle  
503 43r1) for HighResMIP. *Geoscientific model development*, **11**, 3681-3712.

504 Roberts, C. D., R. Senan, F. Molteni, S. Boussetta, S. Keeley, 2017a: ECMWF ECMWF-IFS-LR  
505 model output prepared for CMIP6 HighResMIP. Version 20170915.Earth System Grid  
506 Federation. <https://doi.org/10.22033/ESGF/CMIP6.2463>

507 Roberts, C. D., R. Senan, F. Molteni, S. Boussetta, S. Keeley, 2017b: ECMWF ECMWF-IFS-  
508 HR model output prepared for CMIP6 HighResMIP. Version 20170915.Earth System Grid  
509 Federation. <https://doi.org/10.22033/ESGF/CMIP6.2461>

510 Roberts, M. J., and Coauthors, 2015: Tropical cyclones in the UPSCALE ensemble of high-  
511 resolution global climate models. *Journal of Climate*, **28**, 574-596.

512 Roberts, M., 2017a: MOHC HadGEM3-GC31-LM model o 1008 utput prepared for CMIP6  
513 HighResMIP. Version 20170906.Earth System Grid Federation.  
514 <https://doi.org/10.22033/ESGF/CMIP6.1321>

515 Roberts, M., 2017b: MOHC HadGEM3-GC31-MM model output prepared for CMIP6  
516 HighResMIP. Version 20180818.Earth System Grid Federation.  
517 <https://doi.org/10.22033/ESGF/CMIP6.1902>

518 Roberts, M., 2017c: MOHC HadGEM3-GC31-HM model output prepared for CMIP6  
519 HighResMIP. Version 20170831.Earth System Grid  
520 Federation.<https://doi.org/10.22033/ESGF/CMIP6.446>

521 Roberts, M. J., and Coauthors, 2019a: Description of the resolution hierarchy of the global  
522 coupled HadGEM3-GC313-GC3.1 model as used in CMIP6 HighResMIP experiments.  
523 *Geosci. Model Dev.*, **12**, 4999-5028.

524 Roberts, M. J., 2019b: CMIP6 HighResMIP: Tropical storm tracks as calculated by the TRACK  
525 algorithm. Centre for Environmental Data Analysis, 2019.  
526 <http://catalogue.ceda.ac.uk/uuid/0b42715a7a804290afa9b7e31f5d7753>

527 Roberts, M. J., and Coauthors, 2020: Impact of model resolution on tropical cyclone simulation  
528 using the HighResMIP-PRIMAVERA multi-model ensemble. *Journal of Climate*, **33**, 2557-  
529 2583.

530 Scoccimarro, E., S. Gualdi, G. Villarini, G. A. Vecchi, M. Zhao, K. Walsh, and A. Navarra,  
531 2014: Intense precipitation events associated with landfalling tropical cyclones in response to  
532 a warmer climate and increased CO<sub>2</sub>. *Journal of climate*, **27**, 4642-4654.

533 Scoccimarro, E., A. Bellucci, D. Peano, 2017a: CMCC CMCC-CM2-HR4 model output  
534 prepared for CMIP6 HighResMIP. Version YYYYMMDD[1].Earth System Grid Federation.  
535 <https://doi.org/10.22033/ESGF/CMIP6.1359>

536 Scoccimarro, E., A. Bellucci, D. Peano, 2017b: CMCC CMCC-CM2-VHR4 model output  
537 prepared for CMIP6 HighResMIP. Version YYYYMMDD[1].Earth System Grid Federation.  
538 <https://doi.org/10.22033/ESGF/CMIP6.1367>

539 Scoccimarro, E., G. Villarini, S. Gualdi, A. Navarra, G. Vecchi, K. Walsh, and M. Zhao, 2017c:  
540 Tropical cyclone rainfall changes in a warmer climate. *Hurricanes and Climate Change*,  
541 Springer, 243-255.

542 Scoccimarro E., Gualdi S., Bellucci A. , Peano D., Cherchi A., Vecchi G.A. , Navarra A. 2020:  
543 The typhoon-induced drying of the Maritime Continent. PNAS doi:  
544 10.1073/pnas.1915364117.

545 Shepherd, J. M., A. Grundstein, and T. L. Mote, 2007: Quantifying the contribution of tropical  
546 cyclones to extreme rainfall along the coastal southeastern United States. *Geophysical*  
547 *Research Letters*, **34**.

548 Tang, X., W.-C. Lee, and M. Bell, 2014: A squall-line-like principal rainband in Typhoon  
549 Hagupit (2008) observed by airborne Doppler radar. *Journal of the Atmospheric Sciences*,  
550 **71**, 2733-2746.

551 Taylor, K.E., D. Williamson and F. Zwiers, 2000: The sea surface temperature and sea ice  
552 concentration boundary conditions for AMIP II simulations. In PCMDI Report 60, Program  
553 for Climate Model Diagnosis and Intercomparison, Lawrence Livermore National  
554 Laboratory, 25 pp.

555 Touma, D., S. Stevenson, S. J. Camargo, D. E. Horton, and N. S. Diffenbaugh, 2019: Variations  
556 in the intensity and spatial extent of tropical cyclone precipitation. *Geophysical Research*  
557 *Letters*, **46**, 13992-14002.

558 Van Oldenborgh, G. J., and Coauthors, 2017: Attribution of extreme rainfall from Hurricane  
559 Harvey, August 2017. *Environmental Research Letters*, **12**, 124009.

560 Vecchi, G. A., and Coauthors, 2019: Tropical cyclone sensitivities to CO2 doubling: roles of  
561 atmospheric resolution, synoptic variability and background climate changes. *Climate*  
562 *Dynamics*, **53**, 5999-6033.

563 Villarini, G., J. A. Smith, M. L. Baeck, T. Marchok, and G. A. Vecchi, 2011: Characterization of  
564 rainfall distribution and flooding associated with U.S. landfalling tropical cyclones: Analyses  
565 of Hurricanes Frances, Ivan, and Jeanne (2004). *Journal of Geophysical Research:*  
566 *Atmospheres*, **116**.

567 Villarini, G., R. Goska, J.A. Smith, and G.A. Vecchi, North Atlantic tropical cyclones and U.S.  
568 flooding, *Bulletin of the American Meteorological Society*, 95(9), 1381-1388, 2014a.

569 Villarini, G., and R. F. Denniston, 2016: Contribution of tropical cyclones to extreme rainfall in  
570 Australia. *International Journal of Climatology*, **36**, 1019-1025.

571 Villarini, G., and Coauthors, 2014b: Sensitivity of tropical cyclone rainfall to idealized global-  
572 scale forcings. *Journal of climate*, **27**, 4622-4641.

573 Voltaire, A., and Coauthors, 2019: Evaluation of CMIP6 DECK Experiments With CNRM-  
574 CM6-1. *Journal of Advances in Modeling Earth Systems*, **11**, 2177-2213.

575 Vanniere, B., and Coauthors, The moisture budget of tropical cyclones: large scale environmental  
576 constraints and sensitivity to model horizontal resolution, *Journal of Climate*, 33, 8457-8474.

577 Voltaire, A., 2018: CNRM-CERFACS CNRM-1092 CM6-1 model output prepared for CMIP6  
578 HighResMIP. Earth System Grid Federation.  
579 [http://cera1094www.dkrz.de/WDCC/meta/CMIP6/CMIP6.HighResMIP.CNRM-](http://cera1094www.dkrz.de/WDCC/meta/CMIP6/CMIP6.HighResMIP.CNRM-CERFACS.CNRM1095CM6-1)  
580 [CERFACS.CNRM1095CM6-1](http://cera1094www.dkrz.de/WDCC/meta/CMIP6/CMIP6.HighResMIP.CNRM-CERFACS.CNRM1095CM6-1)

581 Voltaire, A., 2017: CNRM-CERFACS CNRM-CM6-1-HR model output prepared for CMIP6  
582 HighResMIP. Earth System Grid Federation.  
583 [http://cera1098www.dkrz.de/WDCC/meta/CMIP6/CMIP6.HighResMIP.CNRM-](http://cera1098www.dkrz.de/WDCC/meta/CMIP6/CMIP6.HighResMIP.CNRM-CERFACS.CNRM1099CM6-1-HR)  
584 [CERFACS.CNRM1099CM6-1-HR](http://cera1098www.dkrz.de/WDCC/meta/CMIP6/CMIP6.HighResMIP.CNRM-CERFACS.CNRM1099CM6-1-HR)

585 von Storch, J.-S., and Coauthors, 2017: MPI-M MPI-ESM1.2-HR model output prepared for  
586 CMIP6 HighResMIP. Earth System Grid Federation.

587 <http://cera1105www.dkrz.de/WDCC/meta/CMIP6/CMIP6.HighResMIP.MPI-M.MPI-ESM1->  
588 2-HR

589 von Storch, J.-S., and Coauthors, 2019: MPI-M MPI-ESM1.2-XR model output prepared for  
590 CMIP6 HighResMIP. Earth System Grid Federation.  
591 <http://cera1108www.dkrz.de/WDCC/meta/CMIP6/CMIP6.HighResMIP.MPI-M.MPI-ESM1->  
592 2-XR

593 Wang, S. S., L. Zhao, J.-H. Yoon, P. Klotzbach, and R. R. Gillies, 2018: Quantitative attribution  
594 of climate effects on Hurricane Harvey’s extreme rainfall in Texas. *Environmental Research*  
595 *Letters*, **13**, 054014.

596 Wang, Y., K.-H. Lee, Y. Lin, M. Levy, and R. Zhang, 2014: Distinct effects of anthropogenic  
597 aerosols on tropical cyclones. *Nature Climate Change*, **4**, 368-373.

598 Wehner, M. F., and Coauthors, 2014: The effect of horizontal resolution on simulation quality in  
599 the Community Atmosphere Model, CAM 5.1. *Journal of Advances in Modeling Earth*  
600 *Systems*, **6**, 980-997.

601 Wright, D. B., T. R. Knutson, and J. A. Smith, 2015: Regional climate model projections of  
602 rainfall from US landfalling tropical cyclones. *Climate dynamics*, **45**, 3365-3379.

603 Yu, Z., Y. Wang, H. Xu, N. Davidson, Y. Chen, Y. Chen, and H. Yu, 2017: On the relationship  
604 between intensity and rainfall distribution in tropical cyclones making landfall over China.  
605 *Journal of Applied Meteorology and Climatology*, **56**, 2883-2901.

606 Zhang, M., X. Chen, M. Kumar, M. Marani, and M. Goralczyk (2017). Hurricanes and tropical  
607 storms: A necessary evil to ensure water supply? *Hydrological Processes*, **31**, 4414–4428.  
608 <https://doi.org/10.1002/hyp.11371>

609 Zhang, W., and Coauthors, 2015: Improved Simulation of Tropical Cyclone Responses to ENSO  
610 in the Western North Pacific in the High-Resolution GFDL HiFLOR Coupled Climate  
611 Model. *Journal of Climate*, **29**, 1391-1415.

612 Zhang, W., G. Villarini, G. A. Vecchi, and J. A. Smith, 2018: Urbanization exacerbated the  
613 rainfall and flooding caused by hurricane Harvey in Houston. *Nature*, **563**, 384-388.

614 Zhang, W., G. Villarini, G. A. Vecchi, and H. Murakami, 2019: Rainfall from tropical cyclones:  
615 high-resolution simulations and seasonal forecasts. *Climate Dynamics*, **52**, 5269-5289.

616 Zhao, C., Y. Lin, F. Wu, Y. Wang, Z. Li, D. Rosenfeld, and Y. Wang, 2018: Enlarging rainfall  
617 area of tropical cyclones by atmospheric aerosols. *Geophysical Research Letters*, **45**, 8604-  
618 8611.

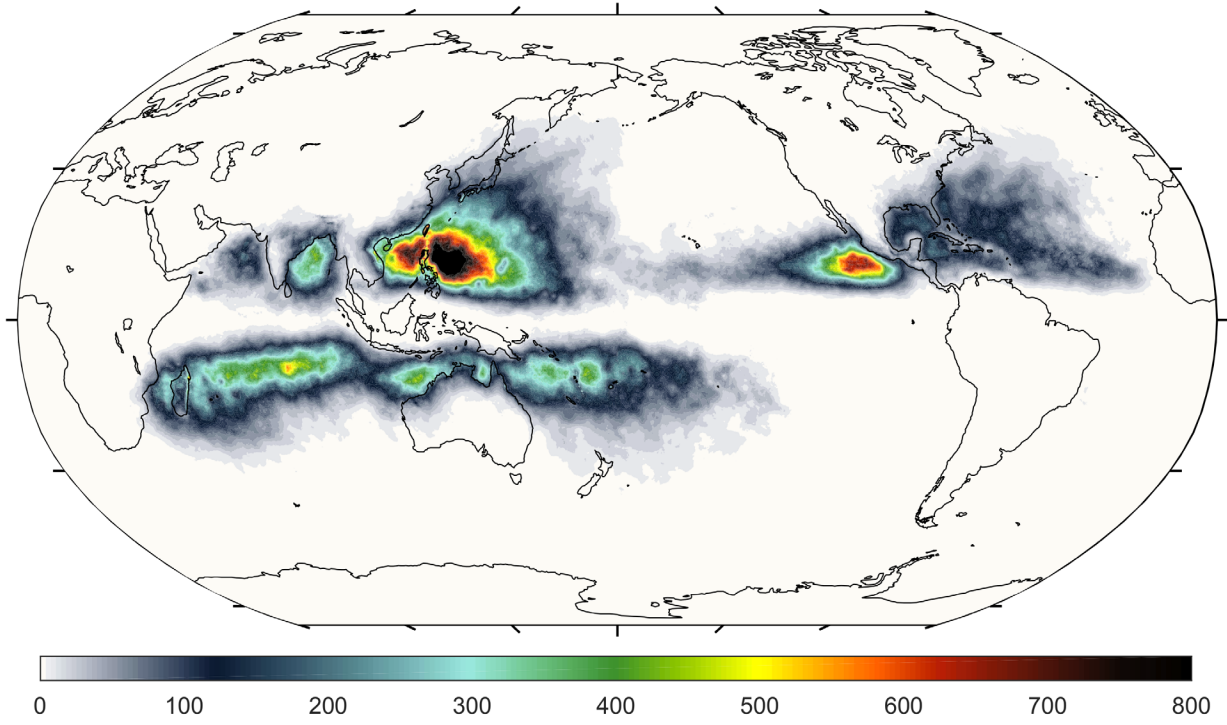
619 Zhao, M., I. M. Held, S.-J. Lin, and G. A. Vecchi, 2009: Simulations of global hurricane  
620 climatology, interannual variability, and response to global warming using a 50-km  
621 resolution GCM. *Journal of Climate*, **22**, 6653-6678.

622

623

624

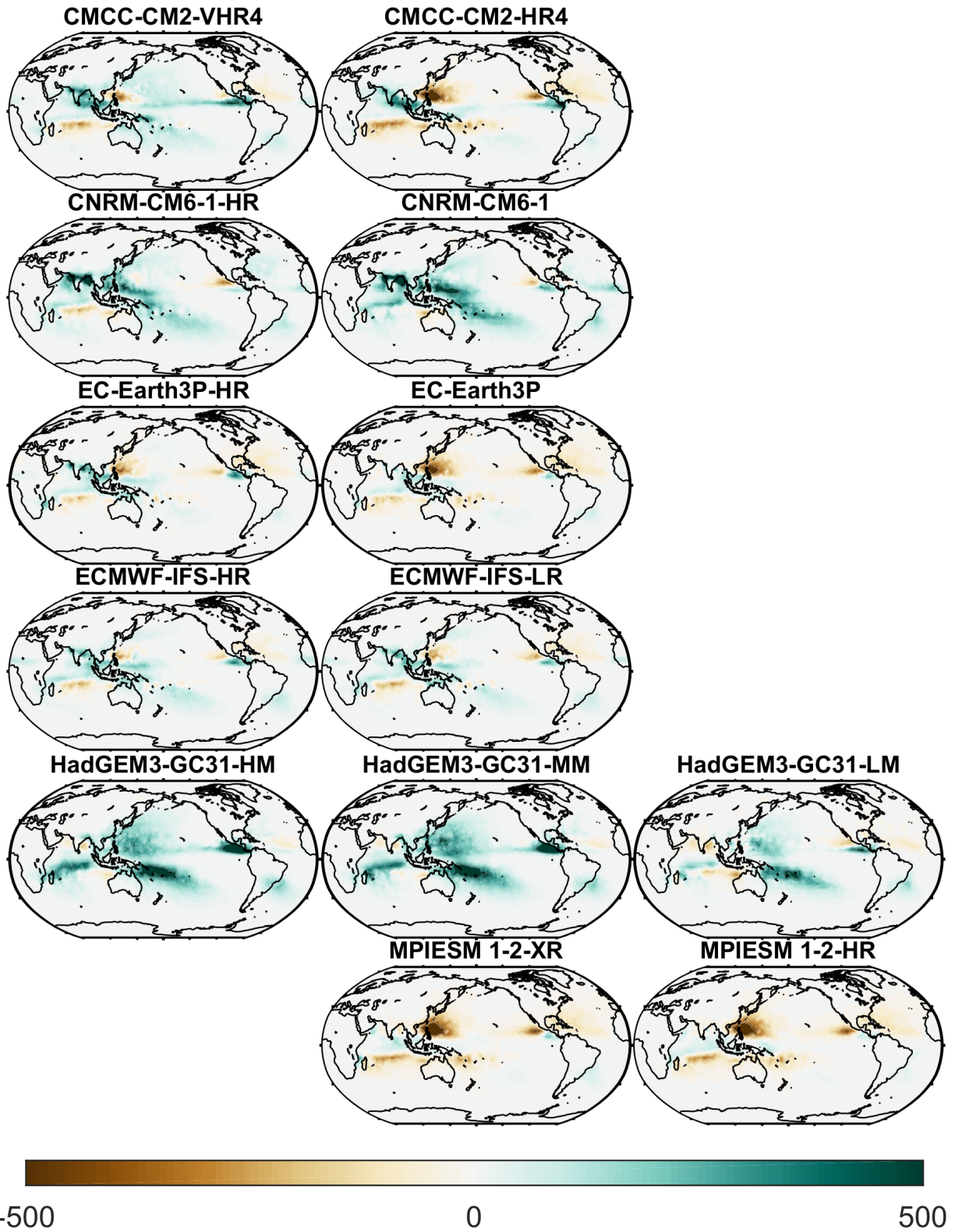
625



626

627 Figure 1 Annual average TC rainfall (unit: mm/year) in observations.

628



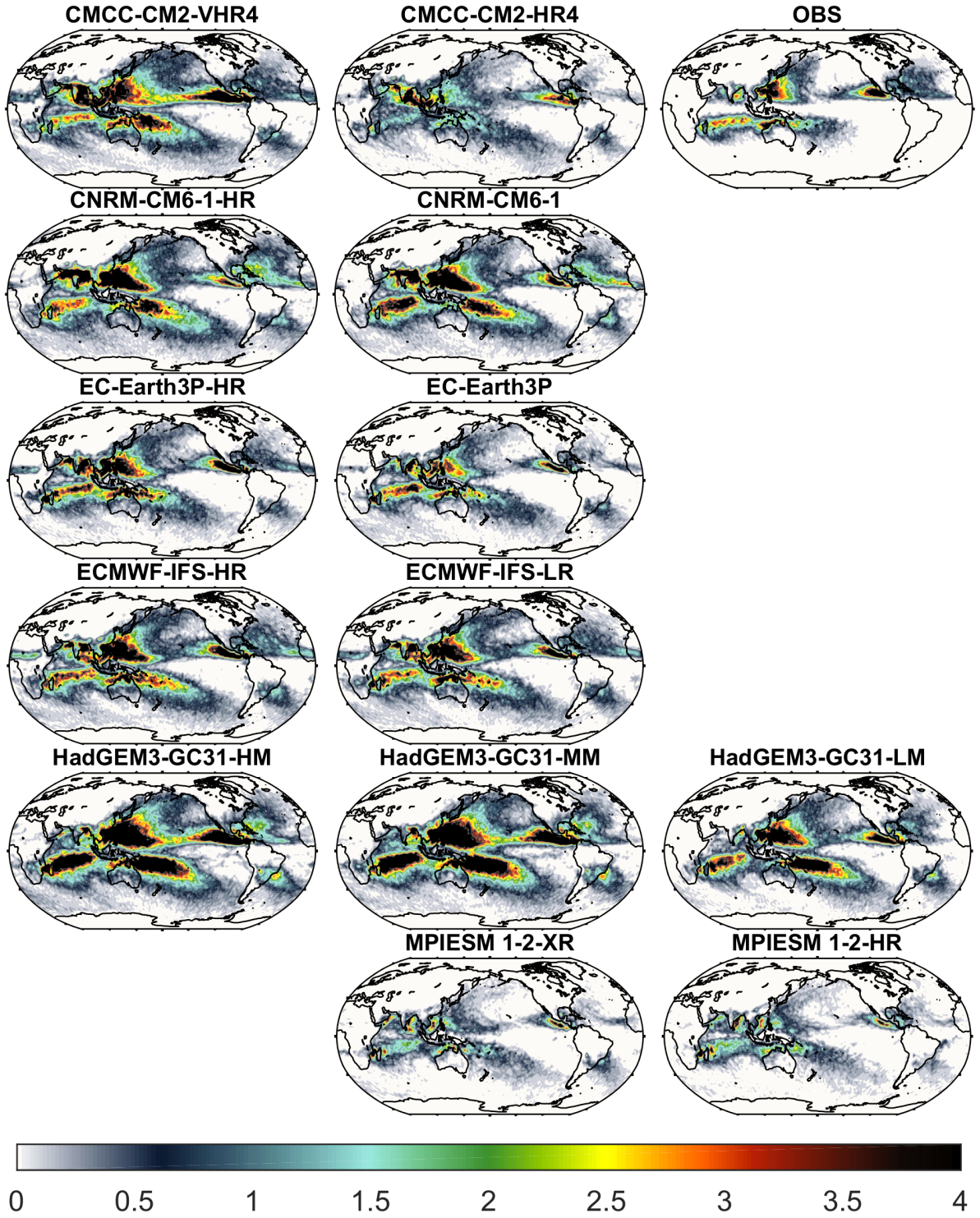
629

630

631

Figure 2. Differences in annual average TC rainfall (unit: mm/year) between observations and climate models archived in the PRIMAVERA Project (model minus observations).



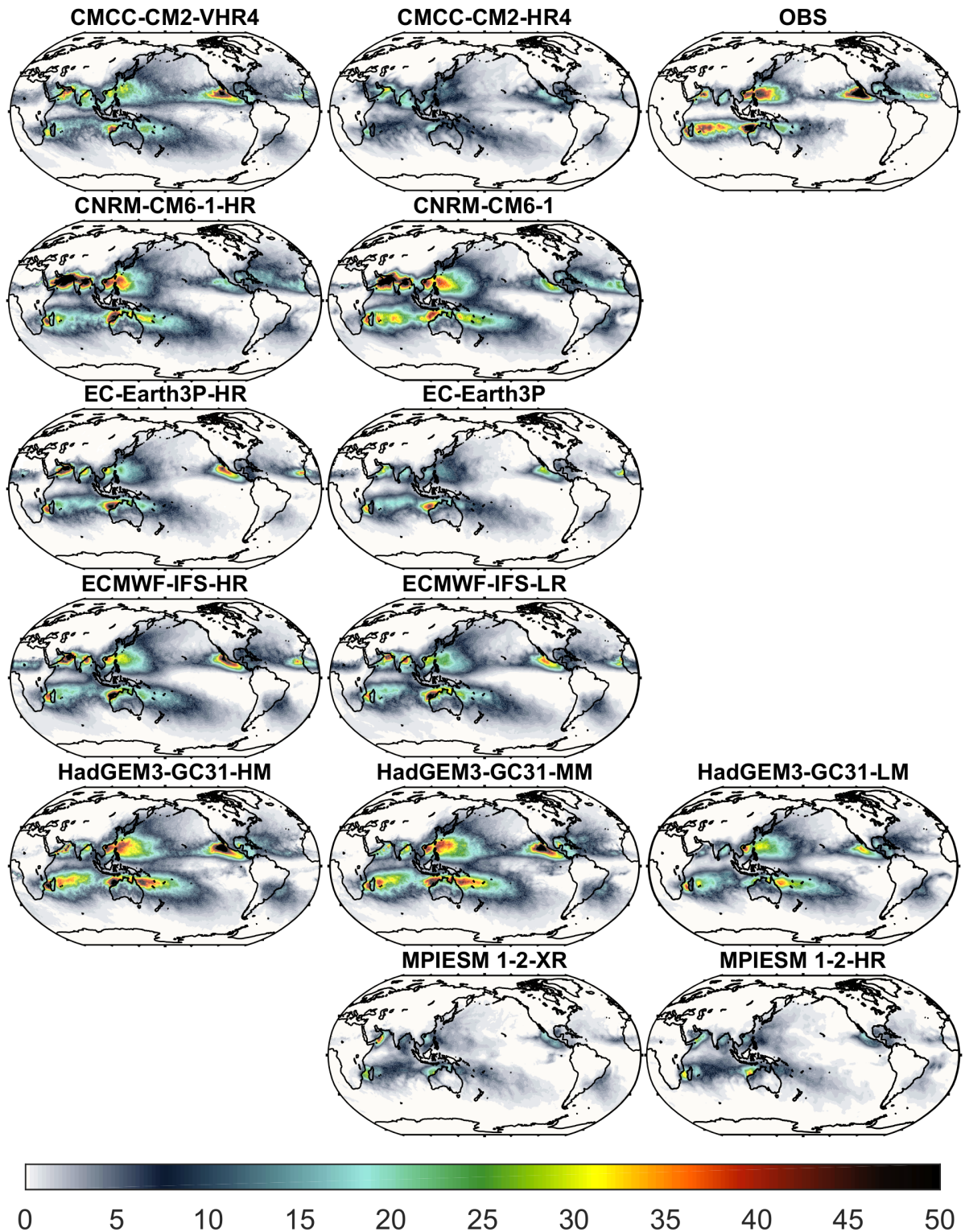


632

633 Figure 3. Annual average TC track density obtained by binning TC tracks into 2×2 spatial  
 634 boxes in observations and climate models archived in the PRIMAVERA Project.

635

636



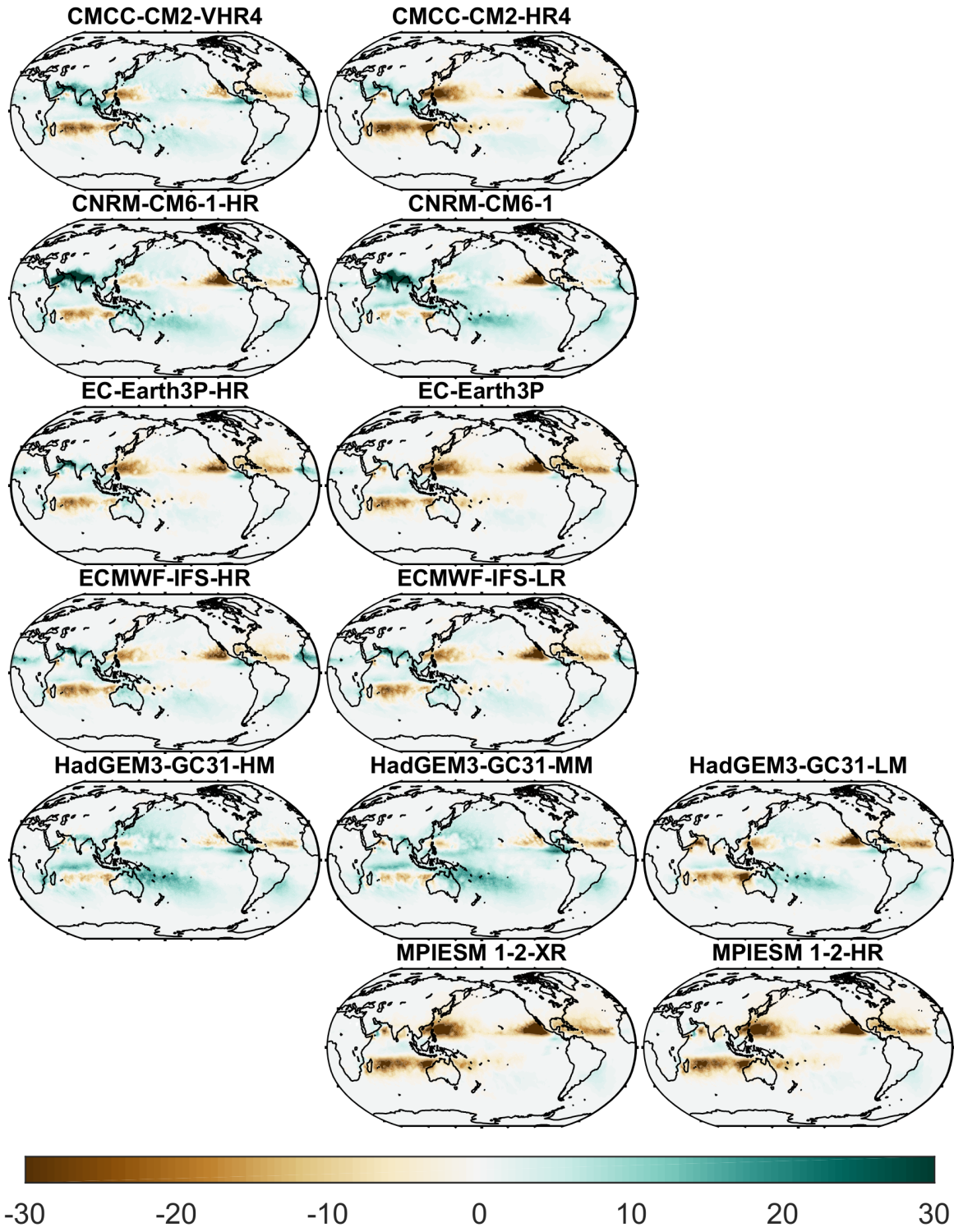
637

638

639

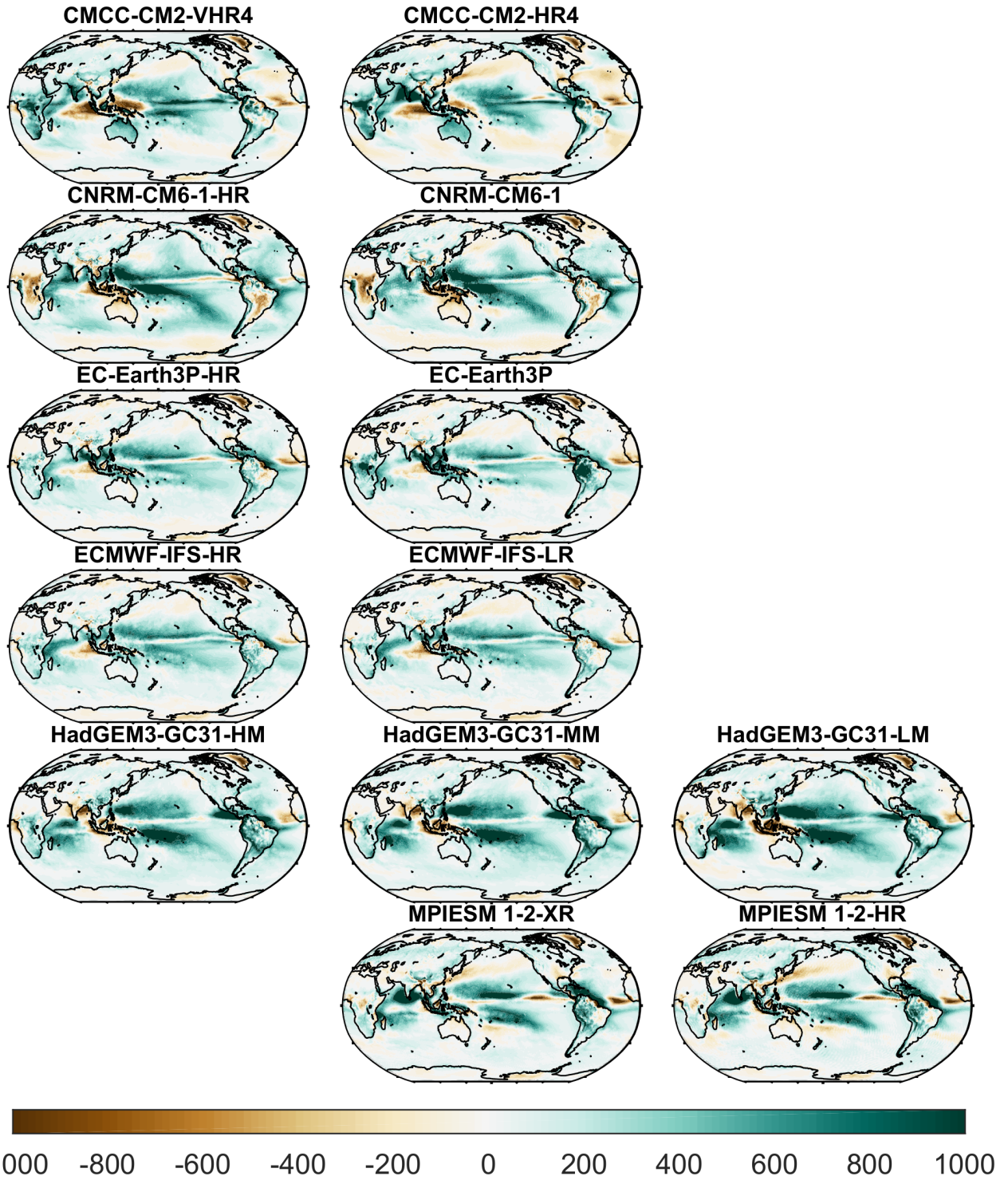
Figure 4. Percentage contribution of TC rainfall to total rainfall (unit: %) in observations and climate models archived in the PRIMAVERA Project.





640  
641  
642  
643

Figure 5. Bias (model minus observations) in the percentage contribution of TC rainfall to total rainfall (unit: %) in the models.



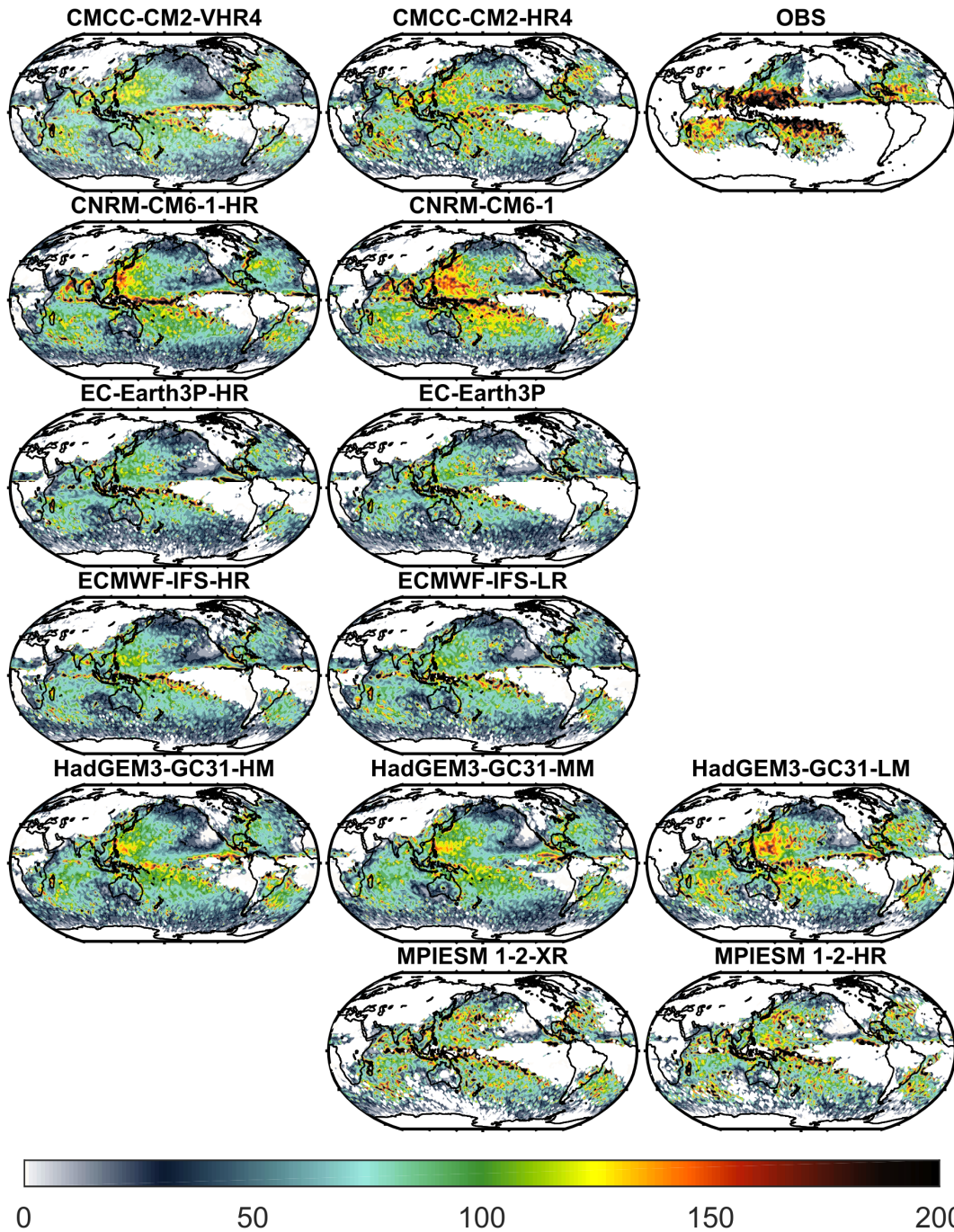
644

645 Figure 6. Bias (model minus observations) in total rainfall (unit: mm/year) in the models.

646

647

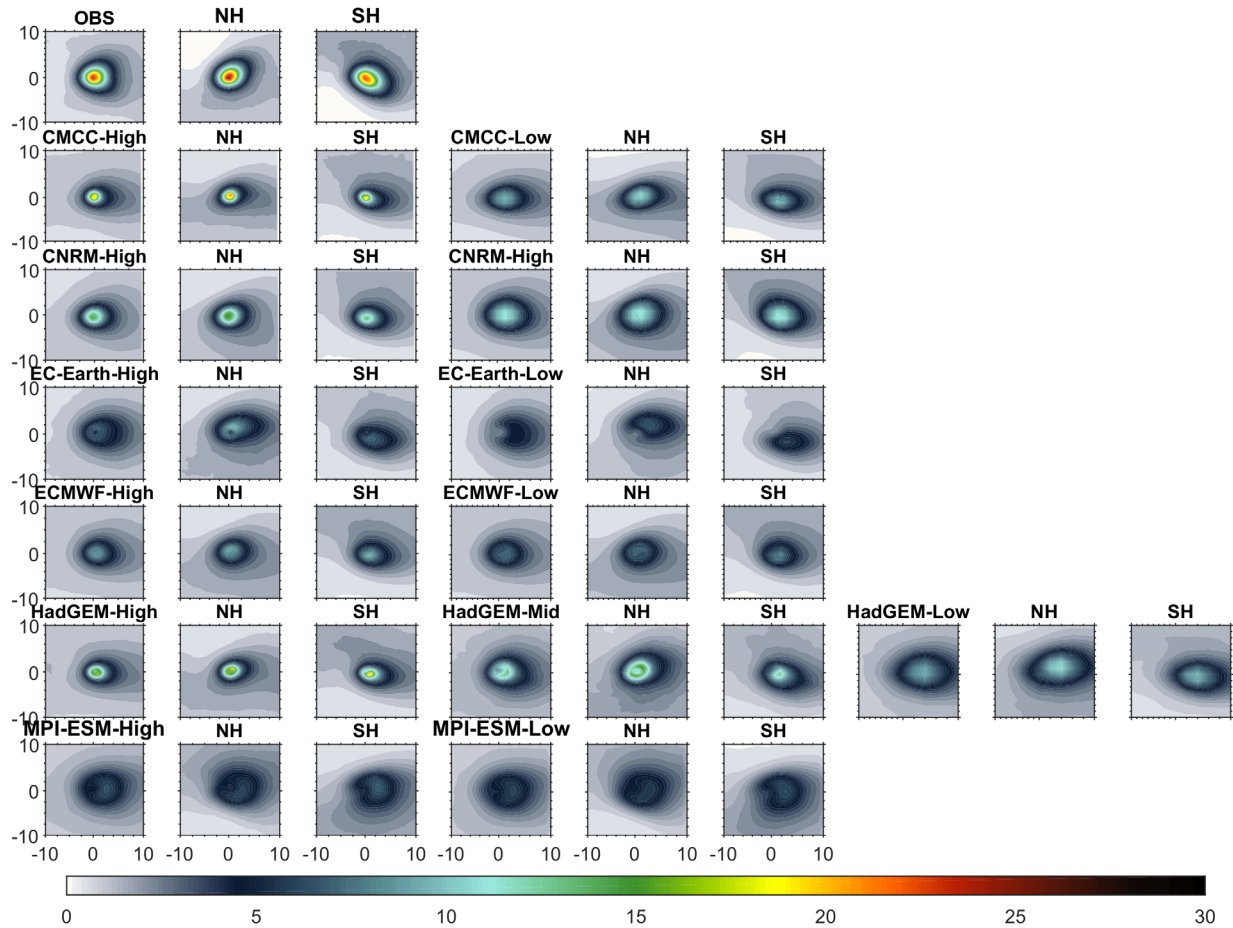




649

650 Figure 7. Average rainfall divided by TC track density (unit: mm) in observations and climate  
 651 models archived in the PRIMAVERA Project. Average rainfall per TC track density represent  
 652 the annual total TC rainfall divided by TC track density obtained by binning TC tracks into  
 653  $2 \times 2$  spatial boxes.

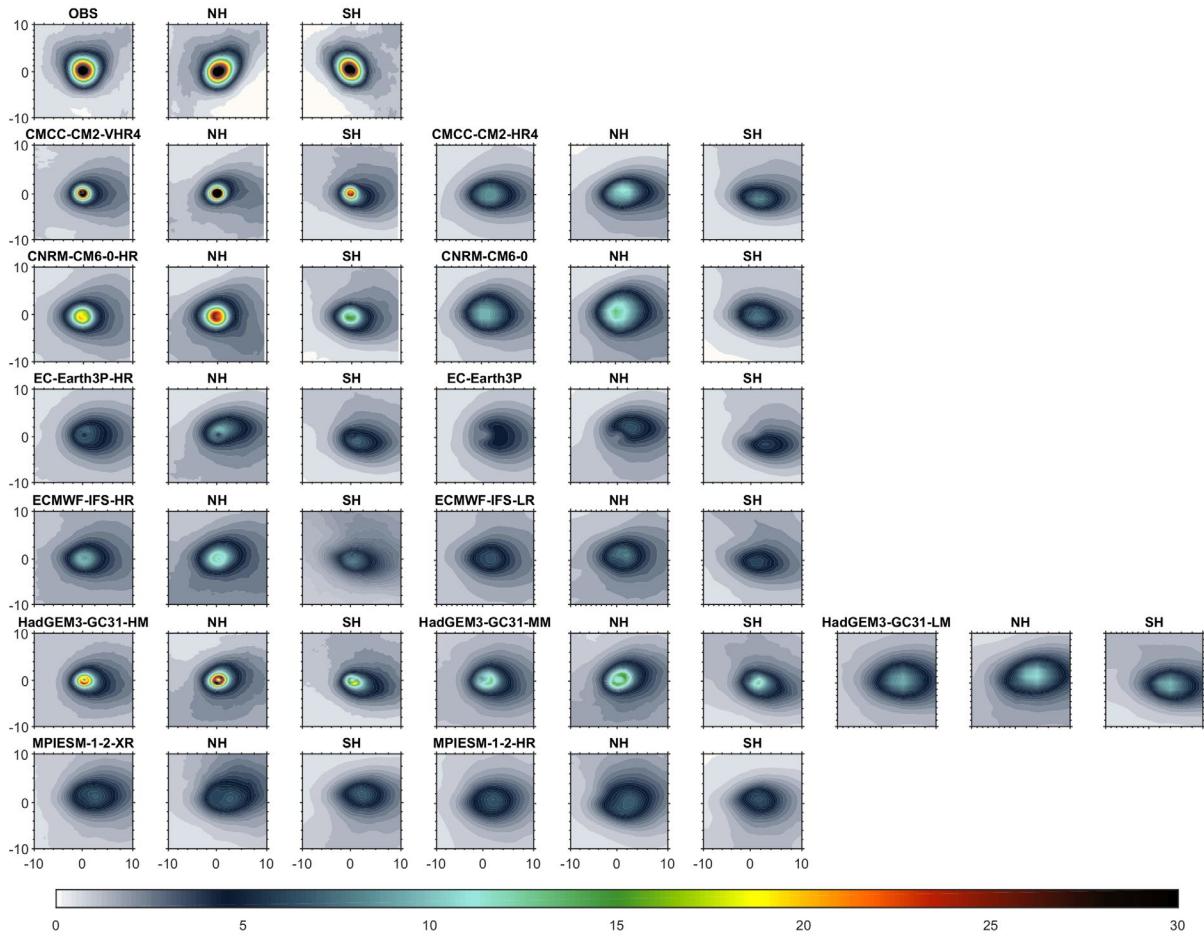
654



656

657 Figure 8. Composite 6-hour TC Rainfall (unit: mm) over the ocean & land in observations and  
 658 climate models archived in the PRIMAVERA Project. The model resolution drops from left  
 659 (columns 1-3) to right (columns 4-6 and 7-9). Every group of three columns represents the  
 660 composite for all the storms, those in the northern hemisphere and those in the southern  
 661 hemisphere.

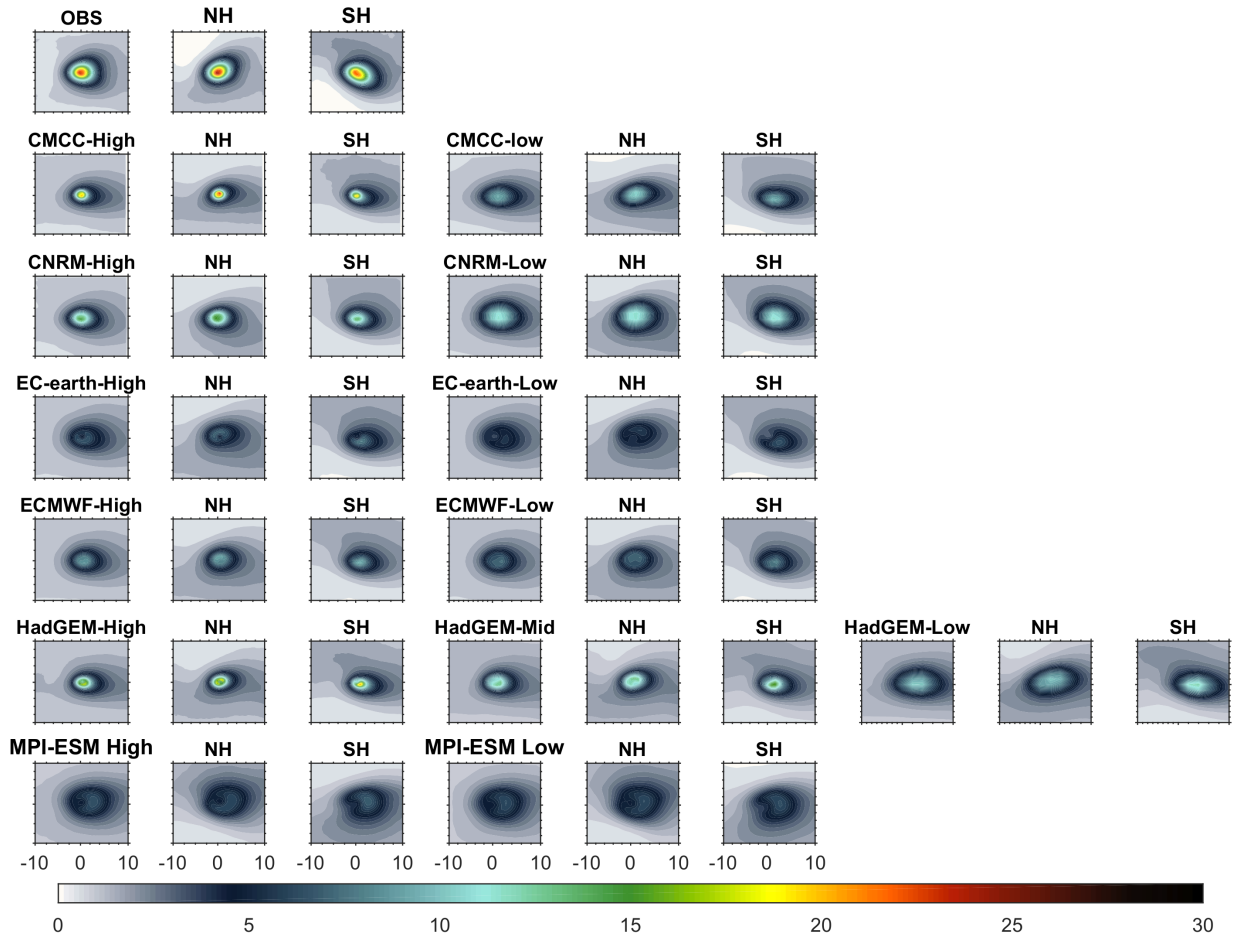
662



663

664 Figure 9. Composite 6-hour TC rainfall (unit: mm) across the 200 TCs with strongest intensity  
 665 (sea level pressure) over the land and ocean in observations and climate models archived in the  
 666 PRIMAVERA Project during 1980-2010. The model resolution drops from left (columns 1-3)  
 667 to right (columns 4-6 and 7-9).

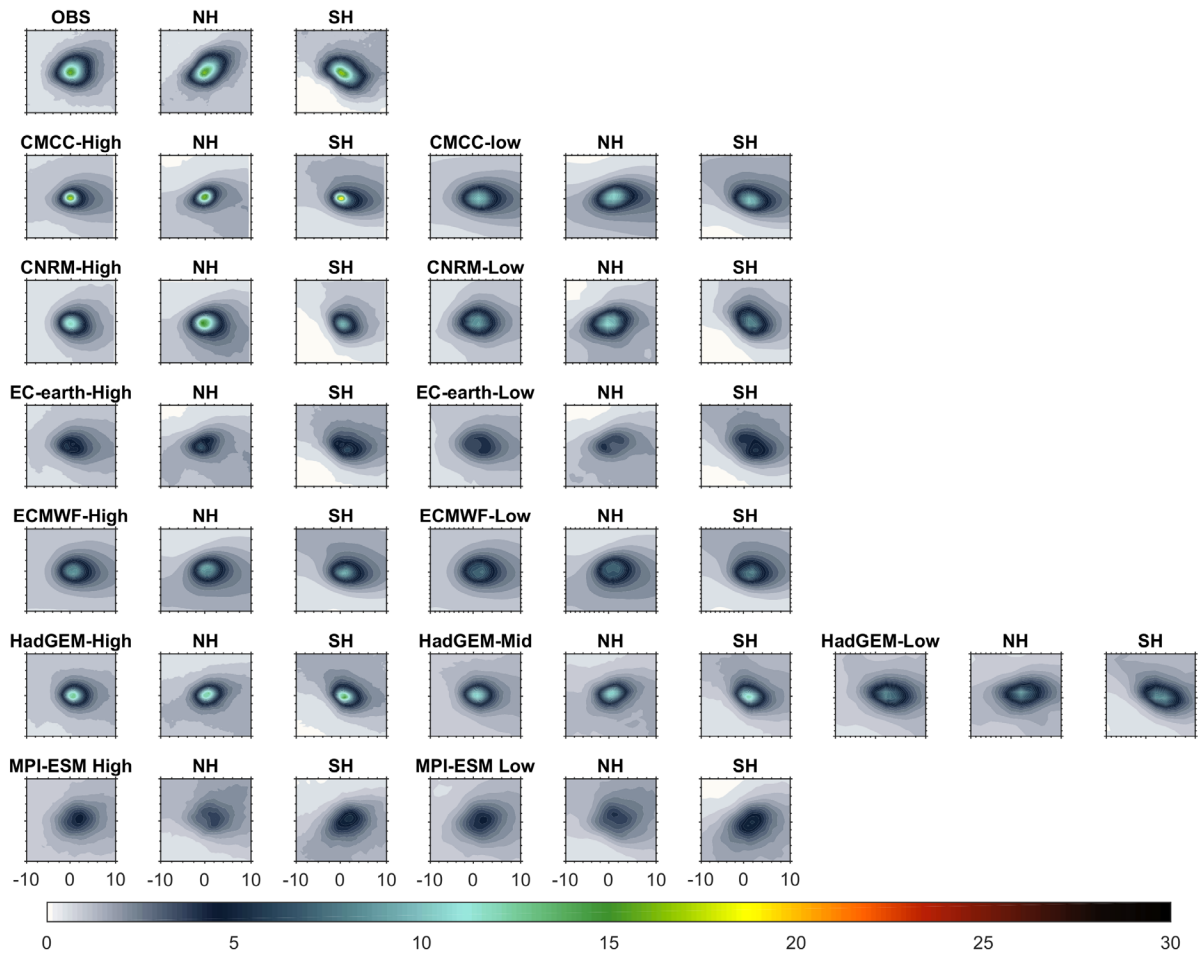
668



669

670

Figure 10. Same as Figure 8 but over ocean.



671

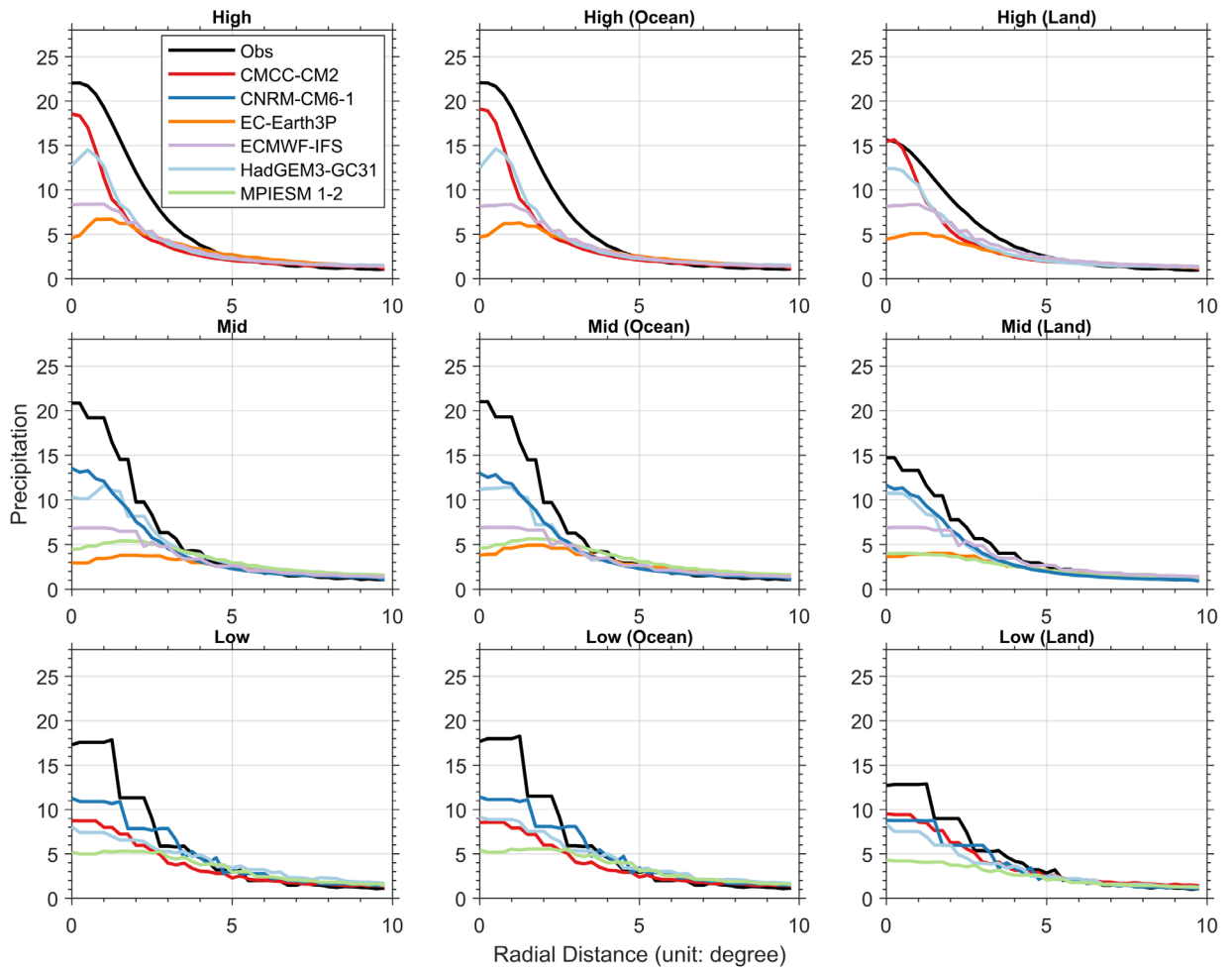
672 Figure 11. Same as Figure 8 but over land.

673

674



675



676

677 Figure 12. Radial profile of composite 6-hour TC rainfall (unit: mm) in observations and  
678 models grouped into high-, mid-, and low-resolution climate models. The spatial resolution of  
679 observed TC rainfall is re-gridded to each group (High, Mid and Low resolution) of the models.

680

681



682 Table 1. Spatial grids of the climate model outputs in high-, middle- and low-resolution groups  
 683 used in this study. While ECMWF IFS data provided to HighResMIP are based on a reduced-  
 684 resolution regular grid, the original ECMWF-IFS output uses the cubic octahedral reduced  
 685 Gaussian grid, with resolutions of Tco399 (~25 km) and Tco199 (~50 km) for the HR and LR  
 686 configurations, respectively.

<b>Model</b>	<b>High</b>	<b>Middle/Medium</b>	<b>Low</b>
CMCC-CM2	1152×768		288×192
CNRM-CM6-1		720×360	256×128
EC-Earth3P	1024×512	512×256	
ECMWF-IFS	720×361	360×181	
HadGEM3-GC313	1024×768	432×324	192×144
MPI-ESM1-2		768×384	384×192

687

688

689

690

691

692

693

694

695

696 Table 2 Definitions of basin boundaries

<b>Basins</b>	<b>Boundary</b>
Western North Pacific (WNP)	0-60°N, 100°E-180
Eastern North Pacific (ENP)	0-60°N, 180-100°W
North Atlantic (NA)	0-60°N, 100°W-0
North Indian Ocean (NI)	0-45°N, 45°E-100°E
South-West Indian Ocean (SI)	0-40°S, 0-90°E
South Pacific & Australia (SP)	0-40°S, 90°E-120°W
South Atlantic (SA)	0-60°S, 60°W-0

697

698

699

700

701

702 Table 3 Correlation between observed and simulated tropical cyclone rainfall across the globe  
 703 and in different basins.

	<b>Globe</b>	<b>WNP</b>	<b>ENP</b>	<b>NA</b>	<b>NI</b>	<b>SI</b>	<b>SP</b>
CMCC-CM2-VHR4	0.77	0.87	0.77	0.68	0.83	0.80	0.76
CMCC-CM2-HR4	0.54	0.62	0.59	0.41	0.77	0.80	0.61
CNRM-CM6-1-HR	0.80	0.94	0.29	0.80	0.70	0.84	0.79
CNRM-CM6-1	0.81	0.89	0.41	0.82	0.74	0.88	0.72
EC-Earth3P-HR	0.85	0.89	0.37	0.77	0.89	0.86	0.90
EC-Earth3P	0.83	0.85	0.33	0.78	0.92	0.88	0.89
ECMWF-IFS-HR	0.87	0.92	0.71	0.79	0.87	0.84	0.85
ECMWF-IFS-LR	0.86	0.92	0.66	0.80	0.88	0.81	0.85
HadGEM3-GC31-HM	0.83	0.94	0.74	0.71	0.62	0.86	0.78
HadGEM3-GC31-MM	0.83	0.93	0.71	0.71	0.70	0.85	0.76
HadGEM3-GC31-LM	0.83	0.94	0.69	0.75	0.76	0.86	0.71
MPIESM 1-2-XR	0.67	0.68	0.26	0.64	0.81	0.73	0.81
MPIESM 1-2-HR	0.71	0.76	0.13	0.75	0.91	0.74	0.82

704

705 Table 4 Root mean square error (unit: mm) between observed and simulated tropical cyclone  
 706 rainfall across the globe and in different basins.

	<b>Globe</b>	<b>WNP</b>	<b>ENP</b>	<b>NA</b>	<b>NI</b>	<b>SI</b>	<b>SP</b>
CMCC-CM2-VHR4	73.39	97.99	61.43	84.63	151.15	64.61	77.94
CMCC-CM2-HR4	79.44	152.37	14.90	80.66	140.61	83.06	74.72
CNRM-CM6-1-HR	95.27	136.22	27.57	46.58	280.06	61.12	67.15
CNRM-CM6-1	106.18	171.88	31.54	53.07	267.48	82.55	80.14
EC-Earth3P-HR	50.48	85.67	14.43	53.69	99.63	54.91	50.96
EC-Earth3P	54.26	125.33	13.08	51.90	40.53	51.50	42.83
ECMWF-IFS-HR	51.28	75.38	16.20	50.56	90.48	58.20	64.27
ECMWF-IFS-LR	49.17	75.97	15.91	44.59	93.09	62.63	61.00
HadGEM3-GC31-HM	129.29	159.11	59.40	161.02	75.63	151.65	143.76
HadGEM3-GC31-MM	130.32	173.13	56.98	151.07	68.51	145.72	147.59
HadGEM3-GC31-LM	76.46	96.64	25.58	62.46	45.38	70.04	96.37
MPIESM 1-2-XR	72.34	171.84	14.29	61.76	43.83	74.66	64.69
MPIESM 1-2-HR	69.57	167.61	14.15	57.32	31.24	72.98	61.12

707

708

709 Table 5 Correlation between observed and simulated tropical cyclone rainfall proportion across  
 710 the globe and in different basins.

	<b>Globe</b>	<b>WNP</b>	<b>ENP</b>	<b>NA</b>	<b>NI</b>	<b>SI</b>	<b>SP</b>
CMCC-CM2-VHR4	0.80	0.86	0.88	0.85	0.71	0.79	0.87
CMCC-CM2-HR4	0.65	0.72	0.71	0.64	0.67	0.79	0.86
CNRM-CM6-1-HR	0.71	0.92	0.55	0.75	0.64	0.85	0.86
CNRM-CM6-1	0.75	0.92	0.53	0.73	0.72	0.93	0.88
EC-Earth3P-HR	0.82	0.91	0.57	0.78	0.80	0.88	0.95
EC-Earth3P	0.81	0.90	0.53	0.72	0.87	0.89	0.95
ECMWF-IFS-HR	0.80	0.93	0.83	0.74	0.78	0.85	0.89
ECMWF-IFS-LR	0.79	0.92	0.79	0.70	0.80	0.82	0.91
HadGEM3-GC31-HM	0.86	0.93	0.78	0.87	0.84	0.88	0.83
HadGEM3-GC31-MM	0.85	0.92	0.71	0.86	0.80	0.88	0.82
HadGEM3-GC31-LM	0.79	0.94	0.67	0.81	0.64	0.90	0.69
MPIESM 1-2-XR	0.69	0.70	0.08	0.64	0.77	0.77	0.89
MPIESM 1-2-HR	0.73	0.77	-0.05	0.67	0.83	0.77	0.93

711

712

713 Table 6 Root mean square error (unit: %) between observed and simulated tropical cyclone  
 714 rainfall proportion across the globe and in different basins.

	<b>Globe</b>	<b>WNP</b>	<b>ENP</b>	<b>NA</b>	<b>NI</b>	<b>SI</b>	<b>SP</b>
CMCC-CM2-VHR4	5.10	5.90	3.41	5.32	9.66	7.93	6.43
CMCC-CM2-HR4	6.58	9.13	2.11	8.61	6.89	9.81	9.88
CNRM-CM6-1-HR	6.57	4.80	2.42	6.98	18.22	6.28	6.69
CNRM-CM6-1	6.26	4.85	2.50	6.97	16.71	4.66	6.14
EC-Earth3P-HR	4.80	6.20	2.41	6.70	7.95	6.47	4.18
EC-Earth3P	5.44	8.59	2.66	8.08	3.73	7.07	5.34
ECMWF-IFS-HR	4.99	4.70	1.77	6.78	8.36	7.26	5.79
ECMWF-IFS-LR	5.03	5.51	1.92	7.49	7.24	7.09	5.03
HadGEM3-GC31-HM	5.14	5.92	3.29	4.92	5.28	6.48	7.99
HadGEM3-GC31-MM	5.14	5.75	3.14	5.14	5.21	5.96	8.26
HadGEM3-GC31-LM	5.10	4.23	2.09	6.82	6.07	5.86	8.78
MPIESM 1-2-XR	6.87	10.79	2.86	9.43	4.82	9.46	9.41
MPIESM 1-2-HR	6.68	10.66	2.90	9.42	4.37	9.23	8.10

715

716

717 **Tropical Cyclone Precipitation in the HighResMIP Atmosphere-only**  
718 **Experiments of the PRIMAVERA Project**

719

720

721 Wei Zhang<sup>1,2\*</sup>, Gabriele Villarini<sup>1</sup>, Enrico Scoccimarro<sup>3</sup>, Malcolm Roberts<sup>4</sup>, Pier Luigi Vidale<sup>5</sup>,  
722 Benoit Vanniere<sup>5</sup>, Louis-Philippe Caron<sup>6</sup>, Dian Putrasahan<sup>7</sup>, Christopher Roberts<sup>8</sup>, Retish Senan<sup>8</sup>,  
723 and Marie-Pierre Moine<sup>9</sup>

724

725

726 <sup>1</sup>IIHR-Hydrosience & Engineering, The University of Iowa, Iowa City, Iowa, USA

727 <sup>2</sup>Department of Plants, Soils and Climate, Utah State University, Utah, USA

728 <sup>3</sup>Fondazione Centro Euro-Mediterraneo sui Cambiamenti Climatici, Bologna, Italy

729 <sup>4</sup>UK Meteorological Office, Exeter, UK

730 <sup>5</sup>National Centre for Atmospheric Science (NCAS), Department of Meteorology, University of  
731 Reading, Reading, UK

732 <sup>6</sup>Barcelona Supercomputing Center (BSC), Barcelona, Spain

733 <sup>7</sup>Max Planck Gesellschaft zur Foerderung der Wissenschaften E.V. (MPI-M), Hamburg, Germany

734 <sup>8</sup>European Centre for Medium-Range Weather Forecasts (ECMWF), Reading, UK

735 <sup>9</sup>Climat, Environnement, Couplages, Incertitudes (CECI), Universit'e de Toulouse, CNRS,  
736 Cerfacs, Toulouse, France

737

738

739

740

741 Table S1 Climatological frequencies of tropical cyclones (January-December, unit: mean  
 742 storms/yr) in the globe and different basins in observations and the climate models.

	<b>Globe</b>	<b>NH</b>	<b>SH</b>	<b>WNP</b>	<b>ENP</b>	<b>NA</b>	<b>NI</b>	<b>SI</b>	<b>SP</b>	<b>SA</b>
Observations	91.6	59.6	32	24.5	19.9	11.9	3.3	14.9	17.1	0
CMCC-CM2-VHR4	148.4	82.8	65.6	33.7	21.3	15.9	11.9	10.3	45.4	9.9
CMCC-CM2-HR4	83.6	48.1	35.5	20.1	7.3	11.4	9.3	6.5	24.1	4.9
CNRM-CM6-1-HR	163	84.8	78.2	40.1	11.3	18.9	14.5	15.6	52.1	10.5
CNRM-CM6-1	167.4	86	81.4	42	13.4	17.6	13	19.7	52	9.7
EC-Earth3P-HR	95.2	48.8	46.4	25	8.2	7.5	8.1	10.5	28.6	7.3
EC-Earth3P	72.7	31.8	40.9	17.2	4.9	4.8	4.9	8.5	25.4	7
ECMWF-IFS-HR	133.1	65.9	67.2	34.7	10.3	12.1	8.8	13	41	13.2
ECMWF-IFS-LR	117.5	58.1	59.4	30.4	9	9.6	9.1	12.3	36.3	10.8
HadGEM3-GC31-HM	206.6	99.7	106.9	43.3	23.6	25.5	7.3	23	69.8	14.1
HadGEM3-GC31-MM	215.4	104.7	110.7	47.3	25.1	24.8	7.5	23.8	73	13.9
HadGEM3-GC31-LM	138.4	63.3	75.1	34.9	12.9	12.3	3.2	16.1	49.7	9.3
MPIESM 1-2-XR	47.3	19.6	27.7	7.8	4.6	3.3	3.9	6	15.6	6.1
MPIESM 1-2-HR	46.9	20.5	26.4	8.6	3.9	4.2	3.8	6.6	15.7	4.1

743

744

745 Table S2 Correlation between observed and simulated tropical cyclone rainfall per TC across the  
 746 globe and in different basins.

	<b>Globe</b>	<b>WNP</b>	<b>ENP</b>	<b>NA</b>	<b>NI</b>	<b>SI</b>	<b>SP</b>
CMCC-CM2-VHR4	0.25	0.09	0.46	0.21	0.25	0.10	0.23
CMCC-CM2-HR4	0.18	0.08	0.22	0.08	0.20	0.09	0.19
CNRM-CM6-1-HR	0.28	0.19	0.46	0.19	0.32	0.03	0.11
CNRM-CM6-1	0.26	0.16	0.36	0.19	0.18	0.04	0.14
EC-Earth3P-HR	0.26	0.16	0.38	0.24	0.22	0.09	0.17
EC-Earth3P	0.28	0.19	0.34	0.23	0.28	0.07	0.27
ECMWF-IFS-HR	0.29	0.20	0.43	0.26	0.28	0.11	0.16
ECMWF-IFS-LR	0.30	0.16	0.47	0.24	0.36	0.09	0.19
HadGEM3-GC31-HM	0.28	0.17	0.38	0.24	0.27	0.18	0.29
HadGEM3-GC31-MM	0.26	0.17	0.47	0.14	0.36	0.11	0.12
HadGEM3-GC31-LM	0.21	0.15	0.50	0.10	0.16	0.02	0.07
MPIESM 1-2-XR	0.17	0.06	0.22	0.17	0.16	0.11	0.17
MPIESM 1-2-HR	0.23	0.11	0.36	0.22	0.26	0.10	0.24

747

748

749

750

751

752

753 Table S3 Root mean square error between observed and simulated tropical cyclone rainfall per  
 754 TC across the globe and in different basins.

	<b>Globe</b>	<b>WNP</b>	<b>ENP</b>	<b>NA</b>	<b>NI</b>	<b>SI</b>	<b>SP</b>
CMCC-CM2-VHR4	122.0	133.0	123.8	87.4	138.7	97.6	126.3
CMCC-CM2-HR4	126.5	133.8	139.1	101.2	137.5	103.3	125.8
CNRM-CM6-1-HR	118.7	128.0	122.0	81.0	131.4	95.3	129.0
CNRM-CM6-1	118.1	127.7	127.1	86.2	137.9	92.7	130.1
EC-Earth3P-HR	126.5	136.4	132.6	87.1	152.7	103.7	128.8
EC-Earth3P	126.8	136.3	143.4	93.3	145.8	102.5	126.0
ECMWF-IFS-HR	122.4	133.1	123.9	86.2	143.3	99.7	129.5
ECMWF-IFS-LR	122.1	133.6	121.6	87.8	137.8	98.7	127.9
HadGEM3-GC31-HM	120.9	130.7	126.8	82.0	148.8	93.4	122.6
HadGEM3-GC31-MM	121.7	130.1	122.4	88.9	141.4	94.8	130.4
HadGEM3-GC31-LM	122.5	128.7	117.0	93.3	151.8	100.8	135.9
MPIESM 1-2-XR	138.4	147.3	149.7	116.2	148.9	111.3	145.0
MPIESM 1-2-HR	129.2	144.3	123.0	91.4	141.5	110.7	138.3

755

756

757 Table S4 Root mean square error and correlation between observed and simulated tropical  
 758 cyclone rainfall across ocean and land.

	<b>Cor (Ocean)</b>	<b>Cor (Land)</b>	<b>RMSE(Ocean)</b>	<b>RMSE(Land)</b>
CMCC-CM2-VHR4	0.79	0.68	66.22	47.32
CMCC-CM2-HR4	0.57	0.51	76.33	36.06
CNRM-CM6-1-HR	0.83	0.67	84.74	64.69
CNRM-CM6-1	0.83	0.62	100.07	57.45
EC-Earth3P-HR	0.86	0.81	48.42	22.17
EC-Earth3P	0.83	0.78	53.15	19.15
ECMWF-IFS-HR	0.88	0.82	47.95	28.07
ECMWF-IFS-LR	0.87	0.83	46.61	24.76
HadGEM3-GC31-HM	0.83	0.79	126.41	48.80
HadGEM3-GC31-MM	0.83	0.80	128.95	40.77
HadGEM3-GC31-LM	0.84	0.83	76.46	18.41
MPIESM 1-2-XR	0.67	0.64	71.22	24.76
MPIESM 1-2-HR	0.72	0.66	68.45	24.08

759

760

761

762

763

764

765

766

767 Table S5 Root mean square error and correlation between observed and simulated tropical  
 768 cyclone rainfall proportion across ocean and land.  
 769

	<b>Cor (Ocean)</b>	<b>Cor (Land)</b>	<b>RMSE(Ocean)</b>	<b>RMSE(Land)</b>
CMCC-CM2-VHR4	0.83	0.69	4.62	3.25
CMCC-CM2-HR4	0.71	0.58	6.45	2.39
CNRM-CM6-1-HR	0.79	0.64	5.27	5.67
CNRM-CM6-1	0.80	0.64	5.42	4.71
EC-Earth3P-HR	0.85	0.74	4.50	2.52
EC-Earth3P	0.84	0.77	5.38	1.62
ECMWF-IFS-HR	0.84	0.71	4.51	3.22
ECMWF-IFS-LR	0.82	0.78	4.78	2.46
HadGEM3-GC31-HM	0.87	0.83	4.85	2.68
HadGEM3-GC31-MM	0.86	0.82	4.89	2.50
HadGEM3-GC31-LM	0.80	0.78	5.04	1.66
MPIESM 1-2-XR	0.70	0.72	6.85	1.86
MPIESM 1-2-HR	0.74	0.74	6.66	1.77

770  
 771  
 772  
 773

774 Table S6 Root mean square error and correlation between observed and simulated tropical  
 775 cyclone rainfall per TC across ocean and land.  
 776

	<b>Cor (Ocean)</b>	<b>Cor (Land)</b>	<b>RMSE(Ocean)</b>	<b>RMSE(Land)</b>
CMCC-CM2-VHR4	0.23	0.22	149.59	119.35
CMCC-CM2-HR4	0.16	0.11	153.68	130.84
CNRM-CM6-1-HR	0.29	0.25	144.20	120.22
CNRM-CM6-1	0.28	0.13	142.20	131.28
EC-Earth3P-HR	0.29	0.19	149.68	134.39
EC-Earth3P	0.25	0.20	157.39	136.33
ECMWF-IFS-HR	0.29	0.19	149.05	121.70
ECMWF-IFS-LR	0.31	0.26	146.64	123.05
HadGEM3-GC31-HM	0.31	0.18	146.65	126.26
HadGEM3-GC31-MM	0.30	0.13	146.91	129.38
HadGEM3-GC31-LM	0.25	0.04	144.65	136.30
MPIESM 1-2-XR	0.17	0.05	163.18	155.18
MPIESM 1-2-HR	0.20	0.17	161.12	145.98

777  
 778